AN ABSTRACT OF THE THESIS OF

Alex R. Long for the degree of Master of Science in Nuclear Engineering presented on June 1 2012.
Title: The Iterative Thermal Emission Monte Carlo Method for Thermal Radiative Transfer.

Abstract approved: _____

Todd S. Palmer

For over 30 years, the Implicit Monte Carlo (IMC) method has been used to solve challenging problems in thermal radiative transfer. These problems are typically optically thick and diffusive, as a consequence of the high degree of "pseudo-scattering" introduced to model the absorption and reemission of photons from a tightly-coupled, radiating material. IMC has several well-known features which could be improved: a) it can be prohibitively computationally expensive, b) it introduces statistical noise into the material and radiation temperatures, which may be problematic in multiphysics simulations, and c) under certain conditions, solutions can be unphysical and numerically unstable, in that they violate a maximum principle – IMC calculated temperatures can be greater than the maximum temperature used to drive the problem.

We have developed a variant of IMC called "iterative thermal emission" IMC, which is designed to be more stable than IMC and have a reduced parameter space in which the maximum principle is violated. ITE IMC is a more implicit method version of the IMC in that it uses the information obtained from a series of IMC photon histories to improve the estimate for the end of time-step material temperature during a time step. A better estimate of the end of time-step material temperature allows for a more implicit estimate of other temperature dependent

quantities: opacity, heat capacity, Fleck Factor (probability that a photon absorbed during a time step is not reemitted) and the Planckian emission source.

The ITE IMC method is developed by using Taylor series expansions in material temperature in a similar manner as the IMC method. It can be implemented in a Monte Carlo computer code by running photon histories for several sub-steps in a given timestep and combining the resulting data in a thoughtful way. The ITE IMC method is then validated against 0-D and 1-D analytic solutions and compared with traditional IMC. We perform an infinite medium stability analysis of ITE IMC and show that it is slightly more numerically stable than traditional IMC. We find that significantly larger time-steps can be used with ITE IMC without violating the maximum principle, especially in problems with non-linear material properties. We also compare ITE IMC to IMC on a two-dimensional, orthogonal mesh, $x - y$ geometry problem called the "crooked pipe" and show that our new method reproduces the IMC solution. The ITE IMC method yields results with larger variances; however, the accuracy of the solution is improved in comparison with IMC, for a given choice of spatial and temporal grid.

The Iterative Thermal Emission Monte Carlo Method for Thermal Radiative Transfer

by

Alex R. Long

A THESIS

submitted to

Oregon State University

in partial fulfillment of
the requirements for the
degree of

Master of Science

Presented June 1 2012
Commencement June 2013

Master of Science thesis of Alex R. Long presented on June 1 2012.

APPROVED:

Major Professor, representing Nuclear Engineering

Head of the Department of Nuclear Engineering and Radiation Health Physics

---

Dean of the Graduate School

I understand that my thesis will become part of the permanent collection of Oregon State University libraries. My signature below authorizes release of my thesis to any reader upon request.

Alex R. Long, Author

ACKNOWLEDGEMENTS

My advisor Dr. Palmer, whose guidance on technical, writing and career issues has been invaluable.

Nick Gentile, my mentor at Lawrence Livermore National Laboratory who taught me so much about radiation transport and building simulations.

My wife Jane who has been a constant source of emotional support. She encouraged me to attend graduate school and has always supported my curiosity and desire to learn.

My parents who've provided love and support throughout my life.

TABLE OF CONTENTS

TABLE OF CONTENTS (Continued)

LIST OF FIGURES

LIST OF FIGURES (Continued)

LIST OF TABLES

The Iterative Thermal Emission Monte Carlo Method for Thermal Radiative Transfer

1 Introduction

All matter radiates energy in the form of photons. The energy of a photon is equal to $h\nu$, where h is Planck's constant and ν is the frequency. The total energy emitted by matter per unit time emitted is proportional to the temperature of the matter to the fourth power. This process is known as radiative heat transfer. The consequence of this fundamental law is that at relatively low temperatures matter does not radiate a significant amount of power. At low temperatures heat transfer is dominated by conduction and convection–the transfer rate for both these mechanisms is proportional to the matter temperature to the first power. At relatively high temperatures, radiative heat transfer is the dominant mechanism for heat transfer. Hot matter emits photons that are then absorbed in the surrounding material. As the surrounding material heats up it emits more photons and this process continues until the energy deposited in the matter is equal to the energy emitted by the matter. If emission and absorption are equal the system is said to be in equilibrium. This mechanism for heat transfer is especially important in very high temperature applications [12]. In astrophysics, the evolution of stars involves extreme temperatures caused by thermonuclear fusion. Likewise, terrestrial fusion power research involves holding high temperature material in a dense configuration for as long as possible. Certain applications of coal power produce high temperatures where radiative transfer needs to be taken into account [10].

Studying the environments and applications where radiative heat transfer is significant is difficult in a laboratory setting because reproducing very high temperatures is dangerous and expensive, and in some cases a violation of international

law. Because of the difficulty associated with performing physical experiments involving radiative heat transfer, high energy density problems are often simulated on digital computers. The radiative heat transfer process can be mathematically described with coupled sets of partial and integro-differential equations. In order to make these equations tractable for computer simulation, assumptions are made about the material properties and the emission process. The equations also need to be discretized. The equations of thermal radiative transfer (TRT) are primarily solved by deterministic methods or Monte Carlo methods. Deterministic methods involve generating the solution (by iteration or direct solution) of a linear system of equations formed from the operators of the TRT equations. Monte Carlo methods involve simulating the life of simulated representative photons by sampling from probability distribution functions with pseudo-random numbers. The life of a simulated particle is called a history. Each simulated photon moves throughout the problem geometry, depositing its energy in the matter. The energy deposited by each simulated photon is tallied to determine the total energy deposited in the matter and, through an equation of state, the new material temperature. Because the material properties are strongly dependent on temperature (the variable being calculated by the simulation), thermal radiative transfer problems are non-linear. A variety of methods (both deterministic and Monte Carlo) exist for solving non-linear problems. These methods are applicable for certain problem conditions, desired accuracy, geometries or available computing power. All of these methods behave differently and they require analysis to ensure that they will work correctly for a desired problem. The stability, accuracy and computational cost of Monte Carlo methods for photon transport is an active area of research.

1.1 Literature Review

This section gives a historical background of the use of the thermal radiative transfer equations and the use of Monte Carlo methods to solve those equations. It also includes an overview of the maximum principle in thermal radiative transfer and the methods that have been proposed to eliminate violations of the maximum principle.

1.1.1 High Energy Density Applications

In 1966, Zel'dovich and Razier [26] discussed the origin of the study of radiative heat transfer: "The theory of radiative heat transfer and radiant heat exchange was created and developed to understand processes which take place in stellar media." The authors add that modern high-temperature applications now require the theory of radiative heat transfer to accurately describe heat transfer in these systems. Zel'dovic and Razier form the equations of thermal radiative transfer and also show how they fit into the hydrodynamic equations but they don't discuss techniques for solving the TRT equations.

Thermal radiative transfer is an essential part of many high energy density systems. Z-pinch experiments use massive currents to create and study plasmas. Most of the energy supplied in Z-pinch experiments is radiated away by the hot plasma [1]. In inertial confinement fusion applications a target is heated with very high energy lasers in an effort to produce fusion within the target. In the National Ignition Facility, a cylindrical object called a hohlraum surrounds the fusion target. The hohlraum is heated by the lasers and then reemits photons that hit the target uniformly; this process is known as an indirect drive system [16]. Research is also ongoing on the redesign of coal power plants to use more oxygen

in the combustion process, which will yield greater efficiency and make it easier to capture greenhouse gases. This is known as oxy-coal combustion. Combustion with oxygen gives a higher flame temperature so radiative heat transfer becomes more important. In their review paper, Scheffknecht et al. [22] stated that "The sub-models identified as being the most relevant to allow the transition to oxy-fuel combustion are the chemical reaction and the thermal radiation models".

1.1.2 Monte Carlo Solutions

The Monte Carlo method as a means to solve particle transport problems was developed by Stanislaw Ulam and John Von Neumann in 1946. The basis of this method is using random numbers to sample from probability density functions to numerically solve the integrals in neutron transport [4]. For example, if there was a source of neutrons uniformly distributed in a basketball in one room of a house and human male in an adjacent room the Monte Carlo method could be used to determine how many neutrons are absorbed in the person's vital organs. To solve the problem random numbers are used to assign a simulated neutron a starting position within the basketball, an angle and a speed. The next location where the neutron will have an interaction is also determined with random numbers. This interaction probability is determined by the material the neutron is passing through. If the neutron scatters its angle is sampled again. If the neutron is absorbed the history is over and a new neutron is created in the basketball. The neutrons that are absorbed in the body contribute to the total energy absorbed. Any total used for calculation in Monte Carlo is called a tally. In order to get an accurate estimate of the amount of radiation absorbed in the person's body many simulated neutrons need to contribute to the absorbed energy tally. This is one

example of how Monte Carlo can be used to solve particle transport.

Monte Carlo methods were initially formulated to solve neutron transport problems but were quickly applied to other problems in physics. In 1963 Fleck [5] first outlined the Monte Carlo method for solving the TRT equations. In this paper he discusses the difference between solving linear and non-linear problems with Monte Carlo and the inability to use the average values from particle histories. This method is explicit in temperature and uses "bundles" of photons as a single simulated photon. The method is compared against finite difference codes that were in use at the time.

In 1971, Fleck and Cummings [6] improved upon Fleck's original method. In their paper they stated that current Monte Carlo methods for radiation transport were limited in both "flexibility and range of applicability." The explicit methods only worked well in optically thin systems and required small time steps in near equilibrium systems and in systems with a relatively large opacities. Fleck and Cummings developed the Implicit Monte Carlo method, which linearizes the TRT equations by expanding the emission temperature with a Taylor series. This procedure introduces an effective scattering term in the radiative energy density equation and multiplies the absorption cross section what is now called the Fleck Factor. This Fleck Factor physically represents the probability that a photon will be reemitted after absorption within the time step. The Implicit Monte Carlo method proved much more useful than the old methods for a wide range of problems.

A few years later, Carter and Forest [2] developed another Implicit Monte Carlo method that samples from an exact solution to the material energy density balance. This method yields an exponential in the total energy emitted and an exponential

distribution in emission time. This method also used opacity and β values from the previous time step to determine the energy emitted and the emission time. The Carter Forest method is more accurate than the IMC method because it solves the material energy balance exactly. The method has not replaced the IMC method because it is more computationally intensive due to the use of logarithms and exponentials as well as the need to use a root solving procedure to determine path-length of photon histories [3].

1.1.3 The Overheating Problem

In IMC simulations where initially cold matter is heated by a radiation field an unphysical overheating of the material can occur. This unphysical overheating is said to violate the "maximum principle", which states that for TRT solutions the temperature should never exceed the highest temperature in the problem. The maximum principle was discussed and quantified by Larsen and Mercier [13] in 1987 for IMC simulations. They prove that for sufficiently small time steps the IMC method will obey the maximum principle. They derive the time-step size limits but they find that the limit is more restrictive than IMC results indicate.

In 2008, Wollaber [25] proposed two methods for correcting the overheating problem: the IMC-T_* method and the time dependent Fleck factor. The IMC-T_* method is based on finding an average temperature, T_*, by solving a deterministic quasi-diffusion calculation that uses information from a preliminary IMC run. An IMC simulation is then run with the temperature dependent properties evaluated at T_*. The time-dependent Fleck factor method (TDF-IMC) is obtained by deriving the IMC equations without making the assumption that the time-step average values are equal to the beginning of time-step values. This time dependent Fleck

factor reduces over heating but also increases run-time because more energy is emitted and effective scattering is increased within a time-step. Wollaber also states that when IMC-T_* and TDF-IMC are used in tandem "substantial suppression in the maximum principle violation..." is achieved.

McClarren and Urbatsch [15] attempt to correct the overheating nature of IMC by integrating the linearized material energy density equation exactly. This produces a different Fleck Factor they call m_∞. This m_∞ factor is always smaller than the Fleck Factor and prevents overheating, but when large time steps are used m_∞ approaches zero and an unphysically small amount of heat is absorbed in the material. They also developed a method to adaptively apply the m_∞ factor if IMC will overheat and apply the normal Fleck Factor if overheating is not expected.

Gentile [8] also introduced a modified Fleck factor to ameliorate overheating in IMC. This modified Fleck factor, g, is derived by including the temperature derivative of opacity when the material energy balance is expanded with a Taylor series. Including the temperature dependence of opacity in the Fleck factor leads to more effective scattering in heating conditions, thus reducing overheating.

Cheatham [3] also showed how including the temperature dependence of opacity can solve the overheating problems . Cheatham employed a predictor-corrector approach, which uses a preliminary IMC simulation to estimate the temperature at the next time step and then updates the opacity using the average temperature for the true IMC simulation. In heating problems, the opacity is often lower at higher temperatures and using this approach, less energy is absorbed. This method does require an initial IMC simulation to determine the new temperature and thus has a potentially increased computational cost.

1.2 Thesis Overview

The remainder of this thesis is organized in the following way:

II. In Chapter 2, the equations for thermal radiative transfer are introduced. Each of the terms in the equations are defined and the non-linear nature of the problem is discussed. Methodologies for solving the equations are discussed as well as some common problems that are used to test new methods.

III. Chapter 3 is devoted to the Implicit Monte Carlo equations. Starting with the thermal radiative transfer equations, the Implicit Monte Carlo equations are derived. The meaning of the Fleck factor is discussed. The section ends with details on the implementation of the IMC equations in a Monte Carlo computer program.

IV. Chapter 4 introduces the Iterative Thermal Emission Implicit Monte Carlo (ITE IMC) method. The ITE IMC equations are derived and the modified terms are identified. The method for modifying a standard IMC code to use the ITE IMC method is discussed.

V. In Chapter 5, the ITE IMC method is verified and tested on common TRT problems. The method is validated against analytic solutions present in the literature and a simple stability analysis is performed for the infinite medium case. Teleportation error is quantified for the ITE IMC method and compared to the standard IMC method. The ITE IMC method is tested on Marshak Wave problems to establish its ability to remedy the overheating present in IMC. The variance and overall figure of merit for the ITE IMC method are calculated.

VI. Chapter 6 contains a discussion of numerical results from the ITE IMC method, and we revisit our research objectives in light of this data. The ITE IMC method is compared and contrasted to the IMC method. Recommendations are made for further analyses and possible improvements are suggested.

2 Thermal Radiative Transfer

2.1 Introduction

The Thermal Radiative Transfer (TRT) equations are described in this chapter. The TRT equations model the physical processes of photon emission and interaction with material. To solve these equations with a computer simulation it is necessary to apply a number of discretizations to the phase space associated with the TRT equations.

2.2 Physical Processes

All matter at a temperature above absolute zero emits photons. Temperature is a measure of the kinetic energy of a group of atoms, so at higher temperatures there is more motion of the atoms or molecules in a material. As the protons and electrons in an atom move they experience different forces and are accelerated. An accelerating charge changes the electromagnetic field and results in the emission of a photon [21]. The total energy emission rate of matter at a temperature T is proportional to T^4. There are a number of different atomic processes that describe the energy a photon generated in a material could have. Within the atom, photons are emitted as electrons move from excited states down to lower energy states. The difference between the higher energy state and the lower energy state is the energy of the emitted photon. If a photon with an energy larger than the binding energy of an electron in an atom interacts with the atom it may eject that electron from the atom. If the photon causing the ejection has an energy greater than the binding energy of the electron the electron will leave with an energy equal to the

difference in the photon's energy and the electron's binding energy. The energy of this electron can take on a continuum of values and when it's absorbed by another atom it will emit a photon from a continuous spectrum. Electrons that are not bound to an atom will also emit radiation as they travel through a material and interact with other charged particles. This emission causes free electrons to lose energy and slow down until they are reabsorbed by an atom or molecule. [26]

In this work the Planckian distribution is used to describe the frequency and intensity of the photons emitted by a material. The Planckian represents matter in an idealized state. The Planckian is:

$$B(\nu, T) = \frac{2h\nu^3}{c^2} \frac{1}{\exp(\frac{h\nu}{kT}) - 1}, \tag{1}$$

where the constants are defined in the following table.

T	=	material temperature
k	=	Boltzmann constant
a	=	Stefan–Boltzmann constant
c	=	speed of light
ν	=	frequency

As the matter emits photons, it loses energy. The total rate of energy loss for the material at a given temperature is equal to Planck function integrated over all frequencies:

$$B(T) = acT^4. \tag{2}$$

All photons interact with the medium they travel through. Photons can be scattered or absorbed by the material. The probability of interacting with a material is described by the material's opacity, usually written as σ. The opacity is the probability of interaction per unit distance. Opacity is a function of the photon's frequency and the temperature of the material.

In order to use relatively simple equations of state to characterize the matter, the assumption of Local Thermal Equilibrium is often made. This assumption states that the properties of the matter are accurately described by its temperature and that the photons are emitted according to the Planck spectrum [25].

2.3 TRT Equations

The TRT equations are derived in detail by Pomraning [19]. The full photon energy balance equation is:

$$\frac{1}{c}\frac{\partial I(x,\nu,\Omega}{\partial t}) + \Omega \cdot \nabla I(x,\nu,\Omega) = S(\nu) - \sigma_a(\nu) I(x,\nu,\Omega) +$$

$$\int_0^\infty d\nu' \int_{4\pi} d\Omega \left[\frac{\nu}{\nu'} \sigma_s(\nu' \to \nu, \Omega' \cdot \Omega) I(x,\nu',\Omega') - \sigma_s(\nu \to \nu', \Omega \cdot \Omega') I(x,\nu,\Omega) \right], \quad (3)$$

where the terms above are defined in the following table:

$I(x,\Omega,\nu)$	=	radiative intensity
$U_m(x,t)$	=	material energy density
$\sigma_a(x,\nu,T,t)$	=	material absorption opacity
$B(\nu,T,t)$	=	Planckian emission

The equations describing the processes in the TRT can be derived in the Eulerian or Lagrangian frame. The specific photon intensity I is the quantity of interest. I is equal to the photon population in a differential element of phase space multiplied by the speed of light, c. The first term is the time rate of change of I within a differential element of phase space. The second term represents the leakage out of a differential element of phase space. The $S(\nu)$ term is a source of photons, it is not necessarily the Planckian but under the LTE assumption it becomes the Planckian distribution. All events that reduce the population of photons are included in the $-\sigma_a(\nu)I(\nu,\Omega)$ term. The last term represents scattering into (the positive term) and out of (the negative term) a differential frequency and solid angle.

The population of photons in a solid angle and frequency effects the probability of photon absorptions and scatters. Interactions that depend upon the current photon population are known as induced processes. This phenomenon is a result of the Pauli Exclusion principle. The probability, P, of an interaction is increased according to:

$$P' = P\left[1 + \frac{c^2 I(x,\nu,\Omega,t)}{2h\nu^3}\right], \tag{4}$$

where P' is the probability accounting for the induced process and the variables I, Ω and ν refer to the population after the event. When Eq. (4) is included in Eq. (3) and the LTE assumption is made the standard TRT equations are formed:

$$\begin{aligned}\frac{1}{c}\frac{\partial I(x,\nu,\Omega)}{\partial t} + \Omega\cdot\nabla I(\nu,\Omega) &= \sigma_a B(\nu,T) - \sigma_a(\nu) I(\nu,\Omega) \\ + \int_0^\infty d\nu' \int_{4\pi} d\Omega \left[\frac{\nu}{\nu'}\sigma_s(\nu'\to\nu,\Omega'\cdot\Omega) I(x,\nu',\Omega')\left[1 + \frac{c^2 I(x,\nu,\Omega,t)}{2h\nu^3}\right]\right] \\ - \int_0^\infty d\nu' \int_{4\pi} d\Omega \left[\sigma_s(\nu\to\nu',\Omega\cdot\Omega') I(x,\nu,\Omega)\left[1 + \frac{c^2 I(x,\nu',\Omega',t)}{2h\nu^3}\right]\right],\end{aligned} \tag{5}$$

In Eq. (5) the source term $S(\nu)$ has been replaced by the Planckian, $B(\nu,T)$. The scattering terms are increased by the induced process term. The Planckian source now includes σ_a', which comes from forcing the equilibrium intensity to satisfy the Planck function [19].

The material energy balance is usually written as:

$$\frac{dU_m(x,T,t)}{dt} = \int^\infty \int^{4\pi} \sigma_a I(x,\nu,\Omega) d\Omega d\nu - \int^\infty \sigma_a B(\nu,T) d\nu + S_m. \tag{6}$$

The first term is the time rate of change of the material energy density, U_m. The photon intensity I from the radiative energy balance in the second term is used to calculate the total energy absorbed in the material over all photon directions

and frequencies. The third term represents the energy loss in the material due to Planckian emission. The last term represents all other possible energy sources into the problem, which may come from other multiphysics processes. The material energy balance and the radiative energy balance are coupled through the I and T terms. The TRT equations very non-linear because the Planckian is not a linear function of temperature. The absorption opacity is often a non-linear function of temperature, adding to the non-linear behavior of the TRT equations. To solve the TRT equations analytically it is necessary to linearize the temperature dependence. This is usually done by evaluating most of the temperature dependent variables at the previous time-step and then using simple expansions for the remaining terms.

2.4 Discrete Equations

In both Monte Carlo and deterministic methods for solving the TRT equations, it is necessary to generate solutions on some kind of spatial grid. Using a spatial grid means that discrete values for the variables of interest can be used instead of continuous functions of position. The frequency ν is also treated in a discrete manner by introducing a series of radiative energy balance equations which each represent a frequency range. These are called the multigroup equations and they are coupled to each other through the scattering terms. If the problem parameters do not depend on frequency, the problem is considered "gray" and one radiative energy balance equation can be used. Another method of dealing with frequency is the one-group method, where parameters are frequency dependent but the radiative energy balance is integrated over all frequencies and yields one equation. In Monte Carlo methods, the photon direction is treated as a continuous variable and is sampled from various distributions. The method for handling the non-linear

nature of the TRT equations is often related to the various methods of time discretization [7]. In deterministic methods, the parameters can be taken at the future time-step and then iterated until convergence. In Monte Carlo methods, the large number of iterations would be very expensive because each iteration would involve simulating many photon histories.

A new method of time discretization is the focus of this thesis. In this thesis only simple orthogonal grids are used to validate new methods. The test problems in this thesis use the gray or single group version of the TRT equations; multigroup test problems were not considered.

2.5 Summary

The TRT equations describe the physical processes of emission and absorption in a material. The equations discretized so they can be implemented on a grid and solved with a deterministic or Monte Carlo method.

3 Implicit Monte Carlo

3.1 Introduction

The thermal radiaitive transfer equations are non-linear in material energy density. Fleck and Cummings put forth a method that linearizes the TRT equations by approximating the emission temperature with a Taylor series. This method is known as Implicit Monte Carlo (IMC). The derivation of the IMC equations and a discussion on implementing the IMC method in a computer program are presented in this section.

3.2 Derivation of IMC Equations

A derivation of the TRT equations in both Eulerian and Lagrangian frames is available in [18]. The standard TRT equations, without scattering and with functional parameters suppressed, are:

$$\frac{1}{c}\frac{\partial I}{\partial t} + \Omega \cdot \nabla I + \sigma_a I = \frac{1}{4\pi}\sigma_a B + S_r, \tag{7}$$

$$\frac{dU_m}{dt} = \int^{\infty}\int^{4\pi} \sigma_a I d\Omega d\nu - \int^{\infty} \sigma_a B d\nu + S_m. \tag{8}$$

Here Eq. 7 represents the radiative energy balance and Eq. (8) represents the material energy balance. The terms above are defined with their functional parameters:

$I(x, \Omega, \nu, t)$	=	radiative intensity
$U_m(x, t)$	=	material energy density
$\sigma_a(x, \nu, T, t)$	=	material absorption opacity
$B(\nu, T, t)$	=	Planckian emission
$S_r(x, \Omega, \nu, T, t)$	=	source to the radiation field
$S_m(x, T, t)$	=	material energy source
c	=	speed of light
ν	=	frequency

When dealing with the TRT equations the variables T_r and T_m are often used to refer to the temperature of radiation field and the material temperature respectively. In this work, T always refers to the material temperature, which is measured in keV. For convenience in deriving the IMC equations the source terms will be left out and reintroduced in the final form. The material energy density, U_m, in terms of temperature and heat capacity, c_V, is

$$U_m = \int_0^T c_V(T) dT. \tag{9}$$

Eqs. (7) and (8) are coupled by the Planckian emission term B, which is a function of frequency and the material temperature:

$$B(\nu, T) = \frac{2h\nu^3}{c^2} \frac{1}{\exp(\frac{h\nu}{kT}) - 1}. \tag{10}$$

The Planckian is often expressed as a function of the equilibrium radiative energy density, U_r, times a probability density function in frequency at a given temperature:

$$B(\nu, T) = b(\nu, T) acT^4 = b(\nu, T) cU_r, \tag{11}$$

$$\int_0^\infty b(\nu, T) d\nu = 1. \tag{12}$$

The integral over frequency in the material energy balance can now be evalu-

ated:

$$\int_0^\infty \sigma_a(\nu,T)B(\nu,T)d\nu = \int_0^\infty \sigma_a(\nu,T)b(\nu,T)acT^4 d\nu = \sigma_{a,p}(T)acT^4, \tag{13}$$

where $\sigma_{a,p}$ is the absorption opacity weighted with the probability density function $b(\nu,T)$:

$$\sigma_{a,p} = \frac{\int_0^\infty \sigma_a(\nu,T)b(\nu,T)d\nu}{\int_0^\infty b(\nu,T)d\nu} = \int_0^\infty \sigma_a(\nu,T)b(\nu,T)d\nu. \tag{14}$$

Substituting Eq. (11) into Eqs. (7) and (8) clarifies the temperature relationship in the TRT equations.

The time derivative in both the radiative energy balance and material energy balance is then approximated by evaluating all temperature dependent properties and the emission temperature at the future time step:

$$\frac{1}{c}\frac{I^{n+1}-I^n}{\Delta t} + \Omega\cdot\nabla I^{n+1} + \sigma_a^{n+1}I^{n+1} = \frac{1}{4\pi}\sigma_a^{n+1}b^{n+1}ca(T^{n+1})^4 \tag{15}$$

$$\frac{U_m^{n+1}-U_m^n}{\Delta t} = \iint \sigma^{n+1}I^{n+1}\,d\Omega\,d\nu - \sigma_{a,p}^{n+1}ca(T^{n+1})^4 \tag{16}$$

This is the first in a series of approximations made with the intent of linearizing the TRT equations. These equations are implicit and their error is $O(\Delta t^2)$ locally and $O(\Delta t)$ globally. The next approximation is made to the material energy balance equation: assuming that the heat capacity c_V is constant over a time step changes the material energy density balance to a temperature update equation:

$$\frac{U_m^{n+1}-U_m^n}{\Delta t} \approx c_V^n\frac{T^{n+1}-T^n}{\Delta t} = \iint \sigma^{n+1}I^{n+1}\,d\Omega\,d\nu - \sigma_{a,p}^{n+1}ca(T^{n+1})^4. \tag{17}$$

Eq. (17) clearly shows how the material energy balance equation is nonlinear in temperature. To linearize this system of equations, the right side of the Eqs. (15)

and (17) are approximated with a Taylor series around the time t^n. In abstract terms, the equations become:

$$\frac{y^{n+1}-y^n}{\Delta t} = F(T^{n+1}) \approx F(T^n) + \Delta t \frac{dF(T)}{dT}\frac{dT}{dt} + O(\Delta t^2). \tag{18}$$

Applying this expansion to Eqs. (15) and (17):

$$\frac{1}{c}\frac{I^{n+1}-I^n}{\Delta t} + \Omega \cdot \nabla I^{n+1} + \sigma_a^n I^{n+1} = \frac{1}{4\pi}\sigma_a^n bca(T^n)^4 + \frac{1}{4\pi}\Delta tca\frac{d\sigma bT^4}{dT}\frac{dT}{dt}, \tag{19}$$

$$c_V^n \frac{T^{n+1}-T^n}{\Delta t} = \iint \sigma^n I^{n+1}\, d\Omega\, d\nu - \sigma_{a,p}^n ca(T^n)^4 - \Delta tca\frac{d\sigma T^4}{dT}\frac{dT}{dt} + O(\Delta t^2). \tag{20}$$

Another set of approximations is then made to evaluate the derivative term in Eqs. (19) and (20). The change in opacity is assumed to be negligible over a time step; this can be a large source of error because opacity can vary as $\frac{1}{T^3}$ (see [8] for treatment of the opacity derivative). $b(\nu, T)$ is also assumed to be constant over the time step– holding $b(\nu, T)$ constant assumes that the frequency distribution of thermally emitted photons does not vary significantly with temperature. After applying these two assumptions, Eqs. (19) and (20) become

$$\frac{1}{c}\frac{I^{n+1}-I^n}{\Delta t} + \Omega \cdot \nabla I^{n+1} + \sigma_a^n I^{n+1} = \frac{1}{4\pi}\sigma_a^n b^n ca(T^n)^4 + \frac{1}{4\pi}\Delta t\sigma^n b^n 4ca(T^n)^3\frac{dT}{dt}, \tag{21}$$

$$c_V^n \frac{T^{n+1}-T^n}{\Delta t} = \iint \sigma^n I^{n+1}\, d\Omega\, d\nu - \sigma_{a,p}^n ca(T^n)^4 - \Delta t\sigma^n 4ca(T^n)^3\frac{dT}{dt}. \tag{22}$$

The material energy balance is now linear in T^n. An expression for the $\frac{dT}{dt}$ term in the radiative energy balance is obtained by solving the material update equation for $\frac{dT}{dt}$ and assuming that $\frac{T^{n+1}-T^n}{\Delta t}$ is equal to $\frac{dT}{dt}$ (an assumption with error $O(\Delta t^2)$). Eq. (22) solved for $\frac{dT}{dt}$ is:

$$\frac{dT}{dt} = \frac{1}{1+\frac{\Delta t\sigma 4ac(T^n)^3}{c_V}}\frac{1}{c_V}\left(\iint \sigma^n I^{n+1}\, d\Omega\, d\nu - \sigma_{a,p}^n ca(T^n)^4\right). \tag{23}$$

Substituting Eq. (23) into the Eq. (21) yields the following:

$$\frac{1}{c}\frac{I^{n+1}-I^n}{\Delta t} + \Omega \cdot \nabla I^{n+1} + \sigma_a^n I^{n+1} = \frac{1}{4\pi}\sigma_a^n b^n ca(T^n)^4$$

$$+\frac{1}{4\pi}\frac{\frac{\Delta t\sigma 4ac(T^n)^3}{c_V}}{1+\frac{\Delta t\sigma 4ac(T^n)^3}{c_V}}\left(\iint \sigma^n I^{n+1} d\Omega d\nu - \sigma^n_{a,p} ca(T^n)^4\right) b^n. \tag{24}$$

It is now convenient to introduce the Fleck factor, f:

$$f = \frac{1}{1+\frac{\Delta t\sigma 4ac(T^n)^3}{c_V}}. \tag{25}$$

Using the Fleck factor, Eq. (24) becomes:

$$\frac{1}{c}\frac{I^{n+1}-I^n}{\Delta t} + \Omega\cdot\nabla I^{n+1} + \sigma^n_a I^{n+1} = \frac{1}{4\pi}\sigma^n_a b^n ca(T^n)^4$$
$$+\frac{1}{4\pi}(1-f)\left(\iint \sigma^n I^{n+1}\, d\Omega\, d\nu - \sigma^n_{a,p} ca(T^n)^4\right) b^n, \tag{26}$$

and simplifies to the standard radiative energy balance in the IMC equations (now using the equilibrium radiation density term $U_r = aT^4$):

$$\frac{1}{c}\frac{I^{n+1}-I^n}{\Delta t} + \Omega\cdot\nabla I^{n+1} + \sigma^n_a I^{n+1} = \frac{1}{4\pi} f\sigma^n_a b^n c U^n_r$$
$$+\frac{1}{4\pi}(1-f) b^n \left(\iint \sigma^n I^{n+1} d\Omega d\nu\right) + S_r. \tag{27}$$

Here the source term S_r is reintroduced, but it is not multiplied by the Fleck factor. The IMC material energy balance equation is:

$$\frac{1}{c_V}\frac{T^{n+1}-T^n}{\Delta t} = f\left(\iint \sigma^n I^{n+1}\, d\Omega\, d\nu - \sigma^n_{a,p} c U^n_r + S_m\right). \tag{28}$$

The source term in the material energy balance is multiplied by the Fleck factor because the whole right hand side is multiplied by the Fleck factor as is shown in Eq. (23).

3.3 Meaning of the Fleck Factor

The Fleck factor ranges between 0 and 1 for all problem parameters. As the length of the time step used in IMC simulations approaches infinity, the Fleck

factor approaches zero. For very small time steps, the Fleck Factor approaches unity. The Fleck Factor is often described as the probability that an absorbed photon is not reemitted within a time step. This is evident from the second source terms in Eq. (27): as f approaches zero, more of the angular intensity, I, will be redistributed according to a Planckian spectrum in energy and isotropically in angle. This physically represents the absorption and reemission of a photon. As f approaches unity, the scattering term vanishes and only absorptions take place. In the material energy balance, the Fleck factor effectively decreases the amount of energy absorbed and the amount reemitted and thus the change in temperature. If the Fleck factor is not used, all absorbed energy in the material would remain there throughout the time step–a non-physical approximation that would lead to an overestimation of material temperature if a large energy source is incident on the material [6].

3.4 Implementing the IMC Equations

In our previous derivations, the IMC equations have not been discussed in a deterministic or Monte Carlo context. They could be solved using either method but they are usually solved via Monte Carlo. The equations can be implemented in a Monte Carlo setting because the intensity can be written as a particle density:

$$I(x, \Omega, \nu, t) = ch\nu N(x, \Omega, \nu, t), \tag{29}$$

where N is the density of simulated photons.

A photon can be simulated in a computer program with the use of pseudo-random numbers and probability density functions. The life of a simulated photon is described in Fig. (1). The simulated photon is assigned a frequency from the Planckian distribution, a random direction vector, a random time of birth (within

the time step) and a random location within a discrete cell. As the photon moves through the problem it will scatter according to an exponential function:

$$p_{scatter} = 1 - e^{-(1-f)\sigma_a x}. \tag{30}$$

To find the distance to scatter, a uniform random variate, ζ, is sampled between 0 and 1 and substituted for $p_{scatter}$ in Eq. (30) [14]. The distance to scatter is then calculated by solving Eq. (30) for x:

$$x = -\frac{1}{(1-f)\sigma_a} \ln(1-\zeta). \tag{31}$$

3.4.1 Non-Analog Monte Carlo

Unfortunately, no computer has the capacity to simulate the actual number of photons present in physical problems. This is not a concern in Monte Carlo neutron transport because the angular flux can be calculated with a source of one neutron and then scaled to the actual problem parameters. This is not possible in thermal radiative transfer because the quantity I depends on the energy of the photon ($h\nu$), not just on the photon density. As a result, a non-analog Monte Carlo procedure is used for photon transport. Each simulated photon represents many real photons: each simulated photon is given a representative energy (sometimes called weight or energy-weight). This energy is distinct from its frequency, which is sampled from the Planckian distribution. The energy of each simulated photon is determined by the number of total photon histories used in the IMC simulation. The number of simulated photons in each discrete spatial zone in the problem is proportional to the energy of that zone:

$$N_{zone} = N_{total} \frac{E_{zone}}{E_{total}}. \tag{32}$$

The same procedure is used for other photon sources:

$$N_{zone} = N_{total} \frac{E_{source}}{E_{total}}. \tag{33}$$

The energy given to each simulated photon is calculated by dividing the total energy of the zone by the number of simulated photons allocated to that zone:

$$E_{photon} = \frac{E_{zone}}{N_{zone}}. \tag{34}$$

In IMC simulations, energy deposition is usually calculated through a procedure called absorption supression [14]. With absorption weighting, the energy absorbed in the material is:

$$E_{abs} = E_{photon}(1 - e^{-f\sigma_a x}), \tag{35}$$

where x is the distance traveled and E_{photon} is the starting energy of the photon. The energy deposited in the material, E_{abs} is added to a tally and after all particles are advanced to the end of the time step the total energy deposited and the total energy emitted in a zone are used with an equation of state to determine the temperature at the next time step.

3.4.2 Census Photons

Simulated photons lose energy as they move through the material in accordance with Eq. (35). It is not practical for the program to track photons of very low energy so at some user determined value, these photons are "destroyed" (deleted from memory). The photons that survive until the end of the time step are placed in census. This means that each of these photons and their energy will carry over to the next time step and be simulated again. They all begin with a time equal to the beginning of the time step, as opposed to emitted thermal photons which are born uniformly at random times within the time step. There are also census

photons on the first time step: this comes from either the radiation in equilibrium with the material (U_r) or from some prescribed initial condition. Census photons are thus created only on the first time step.

3.4.3 Teleportation Error

When a simulated photon is created in IMC it is assigned a random location within a discrete spatial zone. If relatively small time steps are used in conjunction with large spatial zones, energy can travel through the problem at superluminal speeds: this is known as teleportation error. This problem occurs because when a photon deposits its energy in a zone the specific location of this event is not recorded (it is not practical from a computer memory perspective). For instance, if a photon travels a distance x' into a cold zone and reaches census then on the next time step any photons created with a location $x > x'$ will have transported energy faster than the speed of light. This problem stems from the use of discrete spatial zones and leads to an incorrect wave front position in Marshak wave problems. Several attempts have been made to rectify this unphysical characteristic of IMC [3].

3.5 Summary

In this section the IMC equations were derived from the TRT equations. The meaning of the fleck factor and the advantages of effective scattering were discussed. A synopsis was given on solving the IMC equations with a Monte Carlo procedure. The teleportation error associated with Monte Carlo photon simulations was discussed.

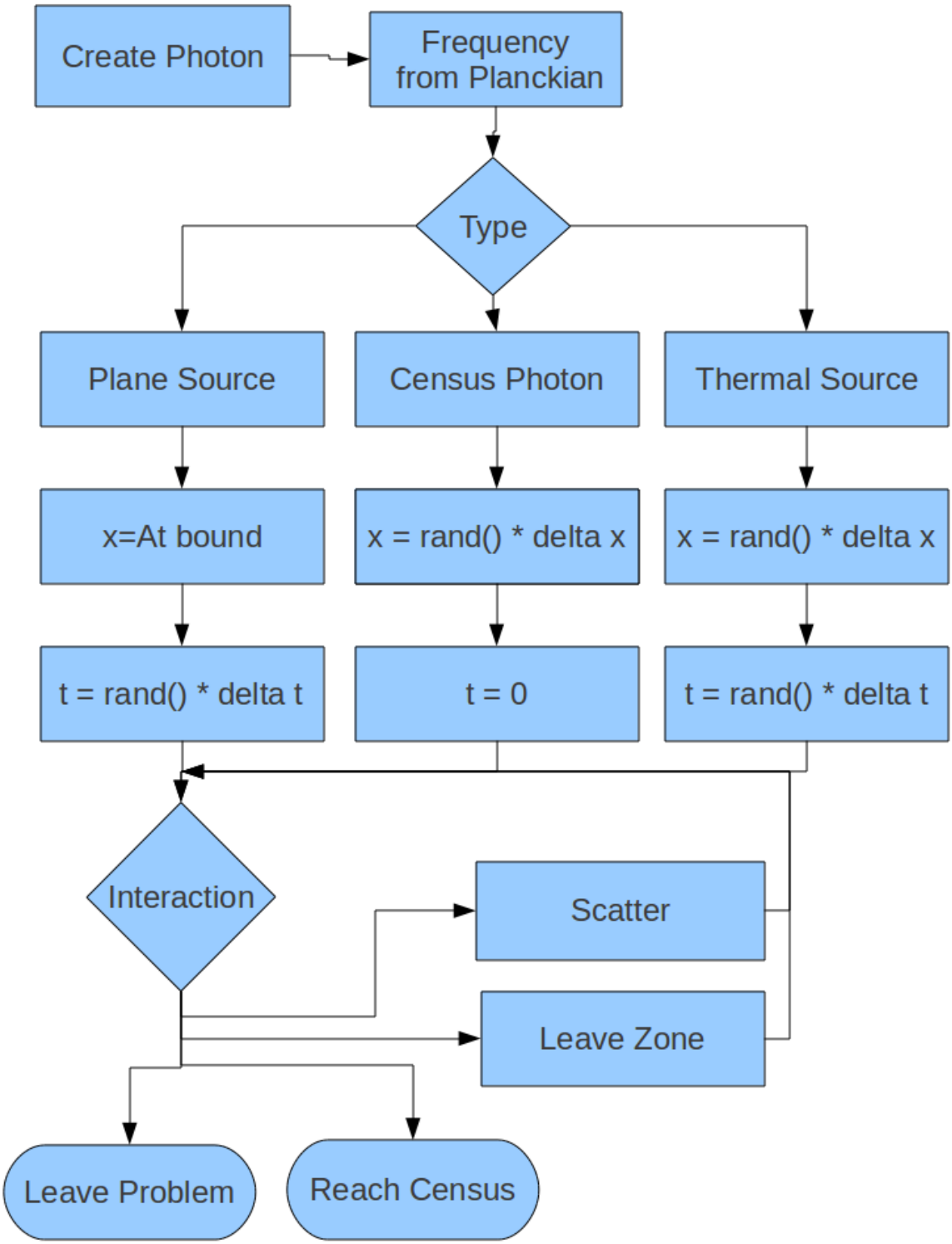

Figure 1: Flow chart describing simulated photon creation and movement (census photons are only created on the first time step)

4 Iterative Thermal Emission IMC

4.1 Introduction

The iterative thermal emission (ITE) version of the IMC equations is derived in this section. A general outline is presented for implementing the ITE IMC method in a Monte Carlo simulation.

4.2 Derivation of the ITE IMC Equations

The standard IMC equations are modified by assuming that the material temperature can be divided into equal portions in a procedure similar to the Rosenbrok method [20]. The material temperature at T^n is:

$$T^n \equiv T_1 + T_2 + ... + T_{N-1}^n + T_N^n = NT_1, \tag{36}$$

where a given "sub temperature" $T_i = \frac{T}{N}$ for $i = 1, 2...N$. The material energy balance for the first sub temperature, T_1, in abstract form is:

$$\frac{dT_1}{dt} = F(T_1^{n+1}) = \frac{1}{N}F(T^{n+1}). \tag{37}$$

The material energy balance for T_1 can be expressed in terms of T because of the relationship in Eq. (36). A Taylor series is used to expand $F(T^{n+1})$ around T^n:

$$\frac{dT_1}{dt} = \frac{1}{N}F(T^{n+1}) \approx \frac{1}{N}\left(F(T^n) + \frac{dF}{dT}\frac{dT}{dt}\Delta t\right) \approx \frac{1}{N}\left(F(T^n) + \frac{dF}{dT}N\frac{dT_1}{dt}\Delta t\right). \tag{38}$$

In Eq. (38) $N\frac{dT_1}{dt}$ is used to represent the $\frac{dT}{dt}$ term. Eq. (38) resembles the standard IMC derivation with a $\frac{1}{N}$ term in front of the emission source. T_1^{n+1} can then be determined from the IMC method using $\frac{1}{N}$ of the source particles.

Now that T_1^{n+1} has been calculated it can be used to obtain a better estimate of T^{n+1} when determining all subsequent values of T_i^{n+1}. This more accurate estimate of T^{n+1} is used in the material energy balance for T_2^{n+1} :

$$\begin{aligned}\frac{dT_2}{dt} &= \frac{1}{N}F(T^{n+1}) \approx \frac{1}{N}\left(F\left(T_1^{n+1}+T_2^{n+1}+(N-2)T_N^{n+1}\right)\right)\\ &\approx \frac{1}{N}\left(F(T_1^{n+1}+T_2^{n}+(N-2)T_N^{n})+\frac{dF}{dT}(N-2+1)\frac{dT_2}{dt}\Delta t\right)\end{aligned} \tag{39}$$

In Eq. (39), the total temperature $\frac{dT}{dt}$ is approximated with $(N-2+1)\frac{dT_2}{dt}$. This represents the derivative of all unknown sub-step values (2 through N). Solving Eq. (39) for $\frac{dT_2}{dt}$ yields:

$$\frac{dT_2}{dt} = \frac{1}{N}F\left(T_1^{n+1}+T_2^{n}+(N-2)T_N^{n}\right)\left(1-\frac{(N-2+1)}{N}\frac{dF}{dT}(T_1^{n+1}+T_2^{n}+(N-2)T_N^{n})\Delta t\right)^{-1} \tag{40}$$

This process is continued until T_N^{n+1} is determined, then the sum of all the energy deposited in each sub-step is used with an equation of state to find T^{n+1}. The equation for a given sub temperature T_i in the ITE IMC method is:

$$\frac{dT_i}{dt} = \frac{1}{N}F(T_{i,N})\left(1-\frac{N-i+1}{N}\frac{dF}{dT}(T_{i,N})\Delta t\right)^{-1}, \tag{41}$$

where

$$T_{i,N} = \left(\sum_{j=1}^{i-1}T_j^{n+1}\right)+(N-i+1)T_i^{n}. \tag{42}$$

The $T_{i,N}$ term is the current estimate for the temperature at the next time step.

Substituting Eq. (41) into the radiative energy balance equation results in the standard IMC equations except with a slightly modified Fleck factor:

$$f_i = \frac{1}{1 + \frac{N-i+1}{N}\beta c\sigma\Delta t}. \tag{43}$$

The Iterative Thermal Emission version of the IMC equations in 1D with 1 frequency group are:

$$c_v \frac{dT_i}{dt} = \sigma_{a,p} \int f_i I_i d\mu + \frac{1}{N}\sigma_{a,p} f_i acT_{i,N}^4 + f_i \frac{1}{N} S_m, \tag{44}$$

$$\frac{1}{c}\frac{\partial I_i}{\partial t} + \mu\frac{\partial I_i}{\partial x} + \sigma_a I_i = \frac{1}{2}\frac{1}{N}\left(\sigma_{a,p} f_i caT_{i,N}^4\right) + \frac{1}{2}\int \sigma_{a,p}(1-f_i) I d\mu' + \frac{1}{N} S_r. \tag{45}$$

The initial condition for intensity is $I_i = \frac{1}{N} I^n$, meaning $\frac{1}{N}$ of the census photons are used for each T_i. c_V, σ and f_i are functions of temperature and use the T^{n+1} estimate at each sub temperature.

After all values of T_i and I_i have been determined by Monte Carlo simulation the material temperature at the next time step, T^{n+1}, is determined by summing the material update equations for each T_i and I_i:

$$T^{n+1} = T^n + \Delta t \left(\sum_{i=1}^{N} \frac{1}{c_{v,i}} \int f_i \sigma_{a,i} I_i d\mu - \sum_{i=1}^{N} \frac{1}{N} \left(\frac{f_i}{c_{v,i}} \sigma_{a,p,i} acT_i^4 \right) \right). \tag{46}$$

4.3 Implementing the ITE IMC Equations

An arbitrary number of iterations can be used in the ITE IMC method. If one step is used the ITE IMC method becomes the standard IMC method. The

main difference in implementation between ITE and IMC is the need to divide the emission energy and the initial census energy by the total number of iterations, N. After dividing by N the problem is run just like an IMC problem. At the end of IMC simulation for a given T_i, Eq. (44) is used to determine the sub temperature. The equation for T_i^{n+1} for a given zone on the mesh is:

$$T_{x,i}^{n+1} = T_{x,i}^{n} + \frac{1}{c_V}\frac{[E_{abs}]}{\Delta x} - \frac{1}{N}\left(\frac{\Delta t}{c_{v,i}} f_i \sigma_{a,p,i} a c T_{i,N}^4\right), \tag{47}$$

where $T_{x,i}$ is the material temperature in a given zone, $T_{i,N}$ is from Eq. (42) and $[E_{abs}]$ is the absorption tally from the IMC simulation. The absorption tally is the total energy absorbed in the zone, the energy density is obtained by dividing the tally by Δx (in more than one dimension it would be divided by the zone's volume). Eq. (42) is then recalculated for this zone and the emission source and the material properties are updated for the next sub-temperature calculation.

The other difference is the need to keep a master list of census photons from all sub-temperature calculations. After all ITE sub-steps have been run the master list is divided up into N smaller lists using random numbers. These smaller lists then serve as the initial condition for each sub-step.

4.4 Summary

The ITE IMC equations were derived by assuming the material temperature can be split into sub-portions. Each sub-temperature can be solved by using the IMC method with a modified Fleck factor. The tracking process is identical to IMC. The major difference between ITE IMC and standard IMC is that the emission temperature and temperature dependent parameters are updated after every ITE sub-step, yielding a more implicit method.

5 Results

5.1 Introduction

In this section the ITE IMC method is verified against analytic solutions from the literature. A stability analysis is performed for the ITE IMC equations in 0-D and the stability of the new method is compared to the stability of IMC. The variance and other sources of error in the IMC and ITE IMC methods are examined and compared. The allowable time steps and grid spacing for Marshak wave problems are determined for the IMC and ITE IMC methods and the "Crooked Pipe" problem is simulated with an ITE IMC code.

5.2 Verification

To demonstrate that the ITE IMC method can accurately solve thermal radiative transfer problems and that the method has been correctly implemented in a computer code, several test problems were run and the results were compared to the analytical solutions available in the literature.

5.2.1 Infinite Medium

Mosher provided a time dependent analytic solution to an infinite medium TRT problem with constant opacitity and heat capacity [17]. This analytic solution is unique because most analytic solutions assume a heat capacity that depends on T^3, which linearizes the TRT equations. A 1-D test problem with reflecting boundary conditions on both ends (an infinite medium), was simulated using the ITE IMC method. For the test problem the constants a and c were both set to 1.0 as well

as the physical parameters σ and c_V. The initial radiation temperature T_r was set to 2.0 and the material temperature T_m was set to 0.001.

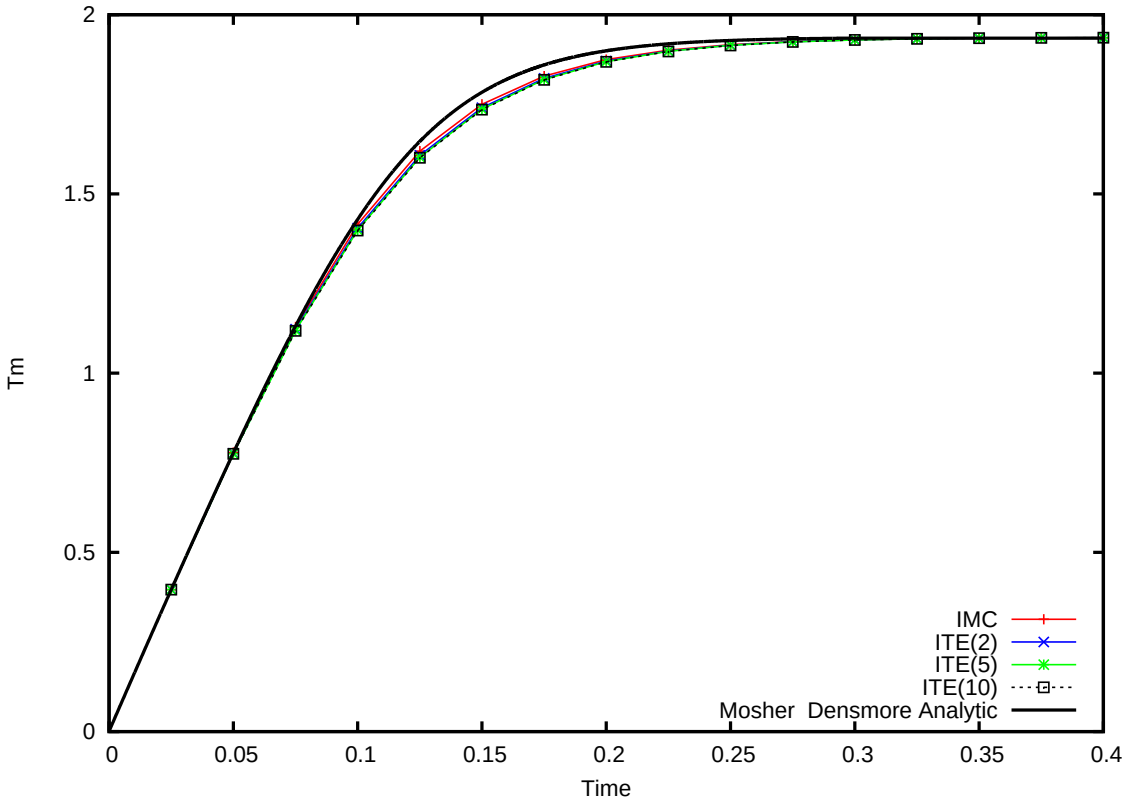

Figure 2: Material temperature vs. time comparing IMC and ITE IMC to the analytic solution

The results in Figures (2) and (3) show that the IMC and ITE IMC method both roughly satisfy the analytic solution with a slightly lower material temperature during the transient. The IMC method is known to absorb less energy than it should in problems where a relatively cold material is heated up by the radiation field [3]. The lower temperature that occurs when more ITE sub-steps are used is

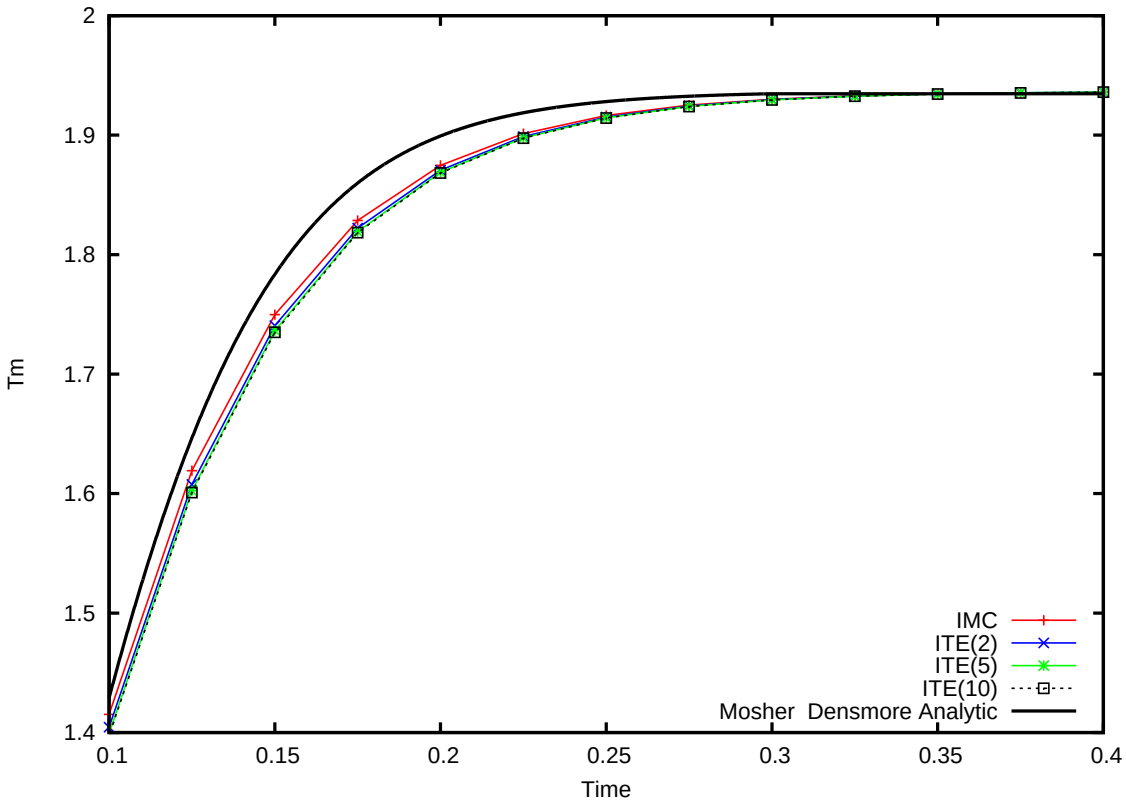

Figure 3: Material temperature vs. position comparing IMC and ITE IMC to the analytic solution near the equilibrium temperature

expected: a more accurate estimate of T_m^{n+1} will be larger thus yielding a smaller Fleck Factor and less overall emission and absorption. Fig. (5) shows that the RMS error approaches zero as the time step is decreased and that the IMC and ITE IMC method are both first order in time.

Fig. (4) shows that the IMC and ITE IMC are equivalent when one sub-step is used in the ITE method.

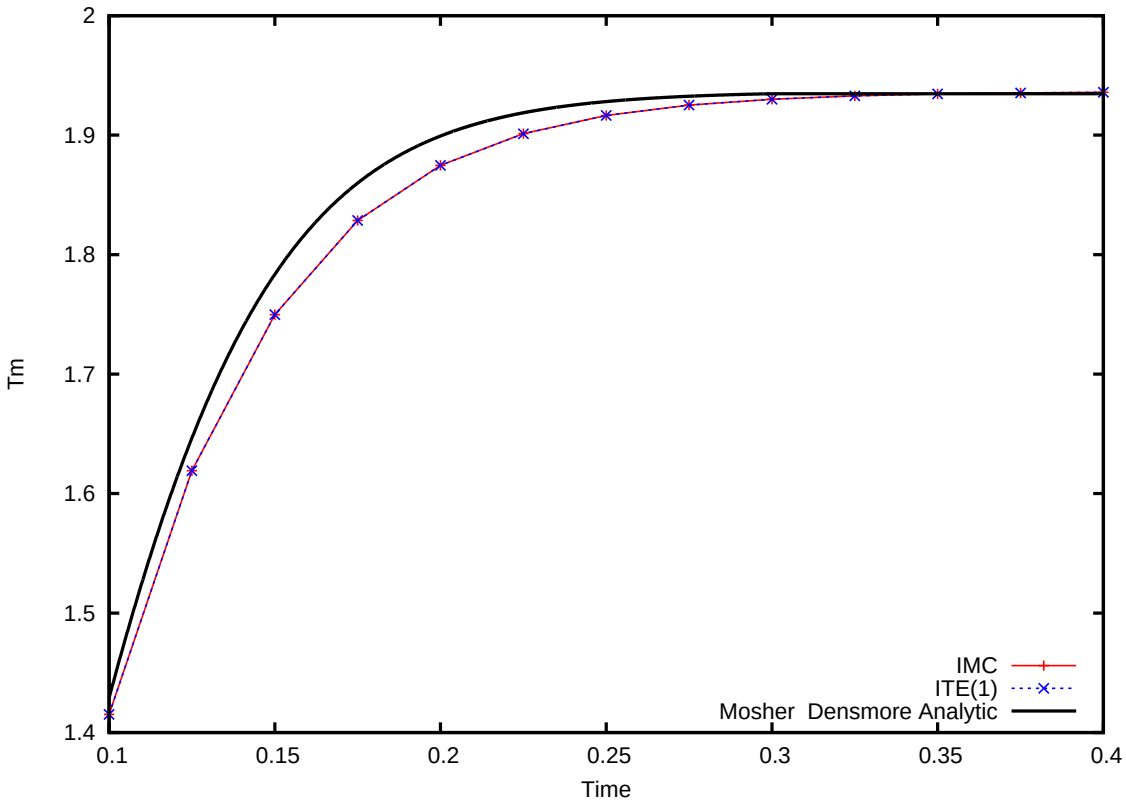

Figure 4: Material temperature vs. position showing the equivalence of IMC and ITE IMC when 1 sub-step is used in the ITE method

5.2.2 1-D

Su and Olson have developed test problems that have long been used to benchmark TRT codes. Their 1997 [23] paper provides the analytic solution for a one-dimensional, time-dependent, linear TRT problem. The TRT equations are linearized by assuming that the heat capacity is proportional to T_m^3, an approximation that was first used by Pomraning [19] and is very useful for obtaining reference solutions. This assumption is not physical but it makes the TRT equations linear

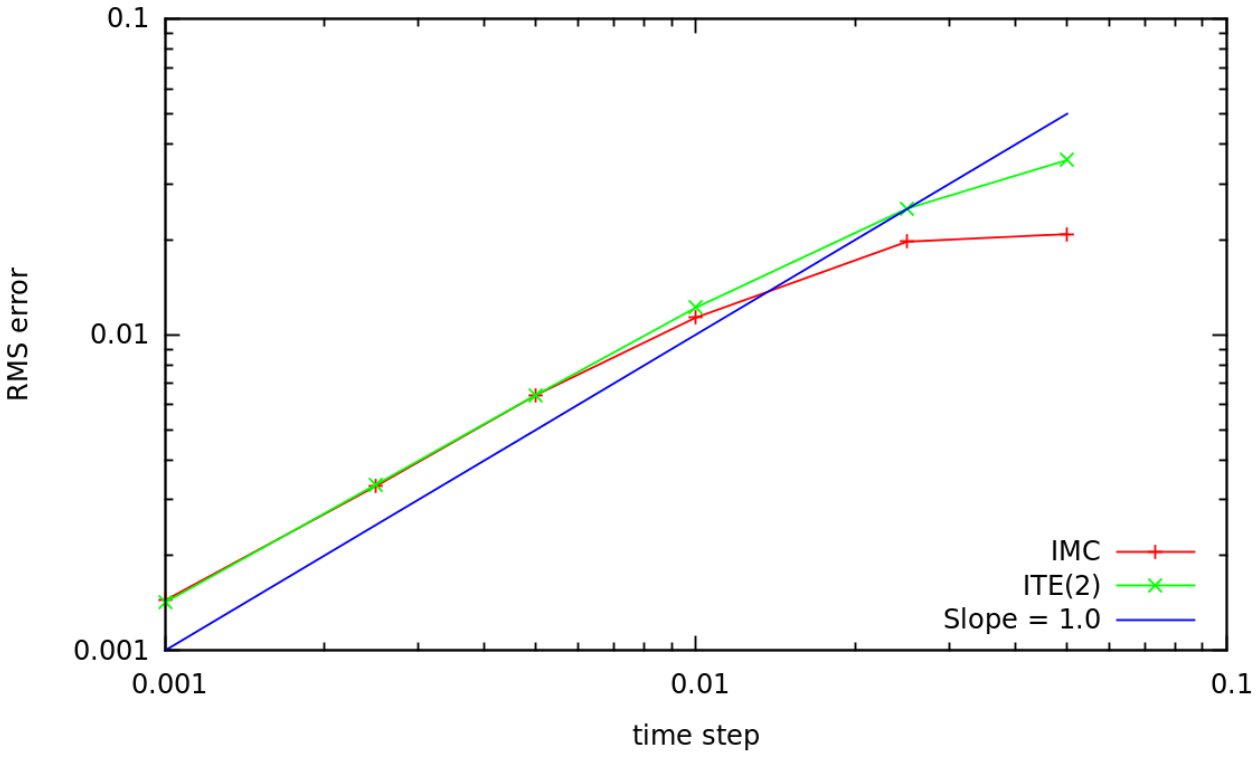

Figure 5: RMS error of IMC and ITE IMC with 2 sub-steps compared to Mosher analytic vs. Δt

in T^4. Both IMC and ITE IMC methods were used to simulate this test problem with $a = c = \sigma = 1.0$ and $c_V = 4.0T_m^3$. In the Su Olson problem, a source of 1.0 (representing radiation coming from material at $T = 1.0$) located between $x = 0$ and$x = 0.5$ is "on" for 10.0 units of time and then turned off. The left boundary is reflecting and the right boundary is a vacuum. Figures (6) through (8) show that the IMC method and the ITE IMC method agree with the analytic solution and with each other. Fig. (9) shows the RMS error for a run with zone centers that correspond to the the x position where the Su-Olson analytic solution is available. The error does not decrease uniformly with smaller time steps due to the error also present from spatial discretization. If the spatial mesh is refined three times the RMS error at $t = 10.0$ with $\Delta_t = 0.05$ is reduced to $7.95E-3$ for the IMC method

and $6.82E-3$ for the ITE IMC method with four sub-steps. This is refinement reduces the RMS error by a factor of two for the same time-step size.

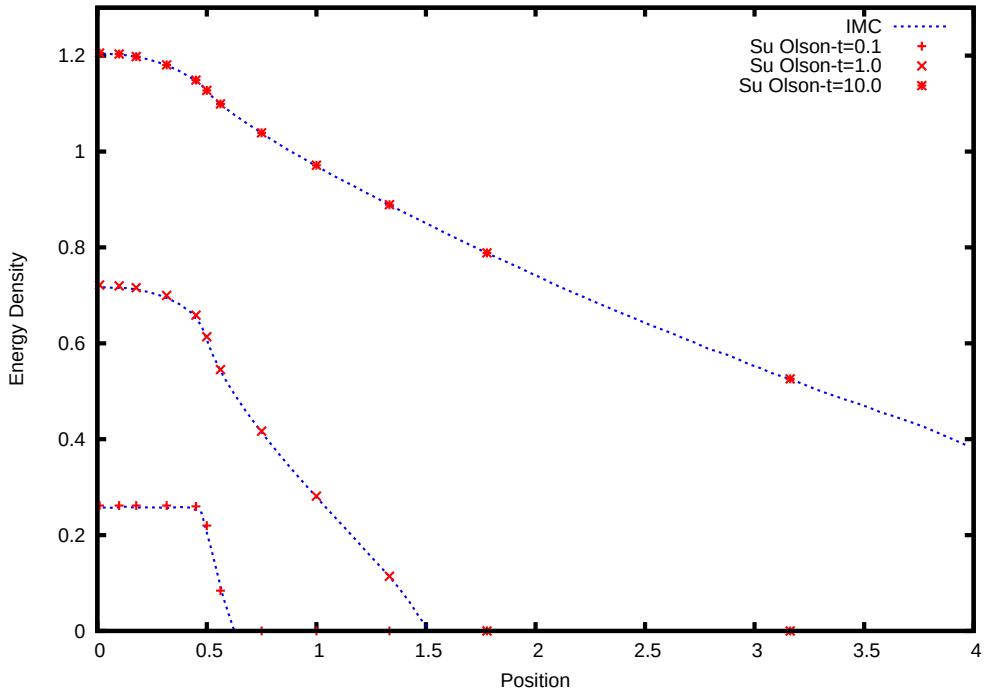

Figure 6: Energy density vs. position comparing IMC to the analytic solution at various times

5.3 Stability Analysis

Mosher and Densmore [24] evaluated the stability of the grey IMC equations in an infinite medium by again assuming that the heat capacity is proportional to T^3. The IMC equations then become a system of equations that can be solved exactly and analyzed by examining the solution at t_{n+1}: the radiation energy density E^{n+1} and the material energy density U^{n+1}. The method of stability analysis used by

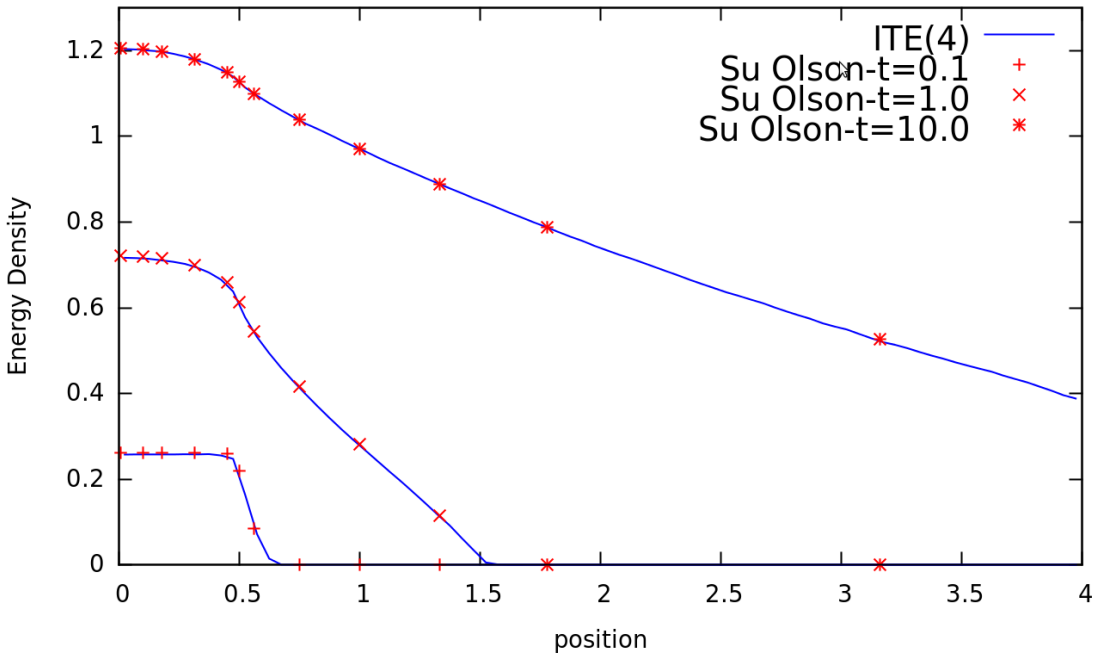

Figure 7: Energy density vs. position comparing ITE to the analytic solution at various times

Mosher and Densmore is applied to the ITE IMC equations: the same assumptions are made and the equations are solved for each sub-step temperature and this information is used in determining the next sub-step temperature. The motivation for solving these equations exactly is finding the eigenvalues of the 2x2 matrix that comes from solving the equations exactly and using a given time step Δt:

$$\begin{pmatrix} E^{n+1} \\ U^{n+1} \end{pmatrix} = \begin{pmatrix} a(\Delta t) & b(\Delta t) \\ c(\Delta t) & d(\Delta t) \end{pmatrix} \begin{pmatrix} E \\ U \end{pmatrix}. \tag{48}$$

The eigenvalues can then be used to determine the amplification for a given time step size Δt.

In this analysis opacity is independent of temperature and the equations are linearized by assuming that the material energy, U, is proportional to T^4:

$$U = bT^4. \tag{49}$$

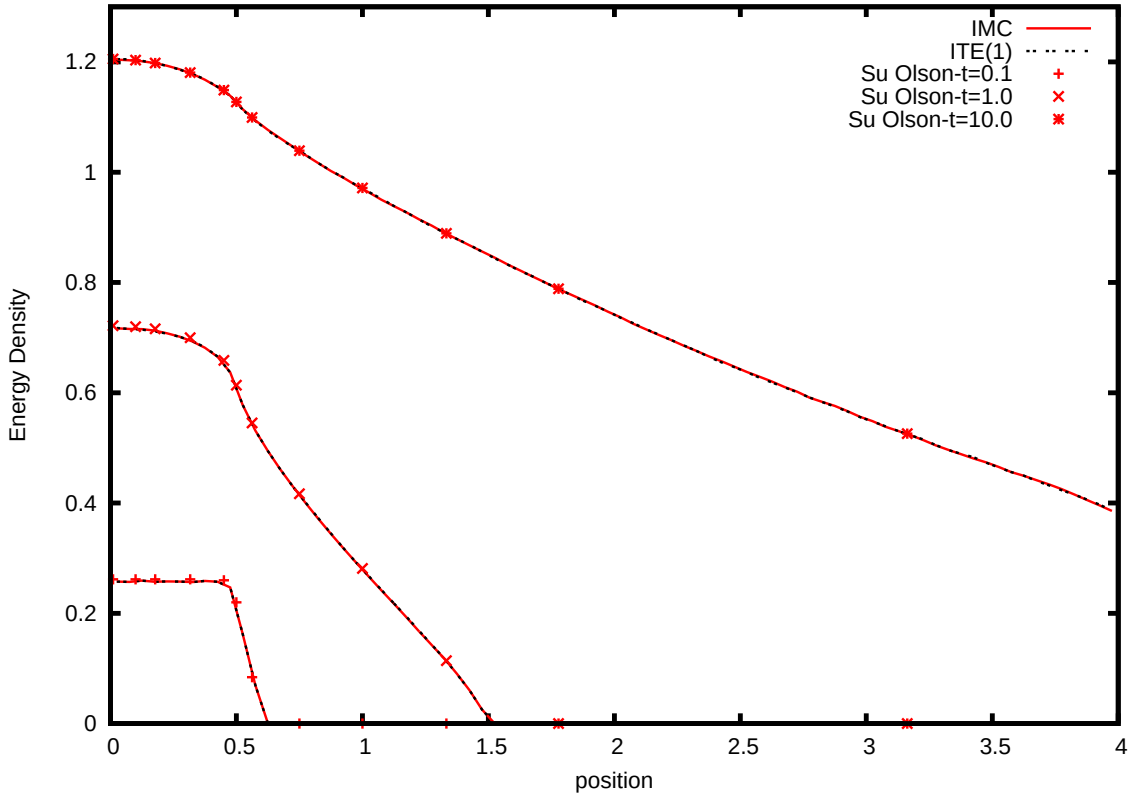

Figure 8: Energy density vs. position showing the equivalence of IMC and ITE IMC when 1 sub-step is used in the ITE method

This is equivalent to the linearization of Pomraning, where heat capacity is assumed to vary with T^3. The assumption in Eq. (49) yields a simple relationship between material energy and the equilibrium radiation density:

$$U_r = aT^4 = \frac{a}{b}U = \beta U \tag{50}$$

The standard 0-D IMC equations in the standard backward Euler form are:

$$\frac{dE}{dt} + f_n\sigma_n cE = f_n\sigma_n cU_r^n, \tag{51}$$

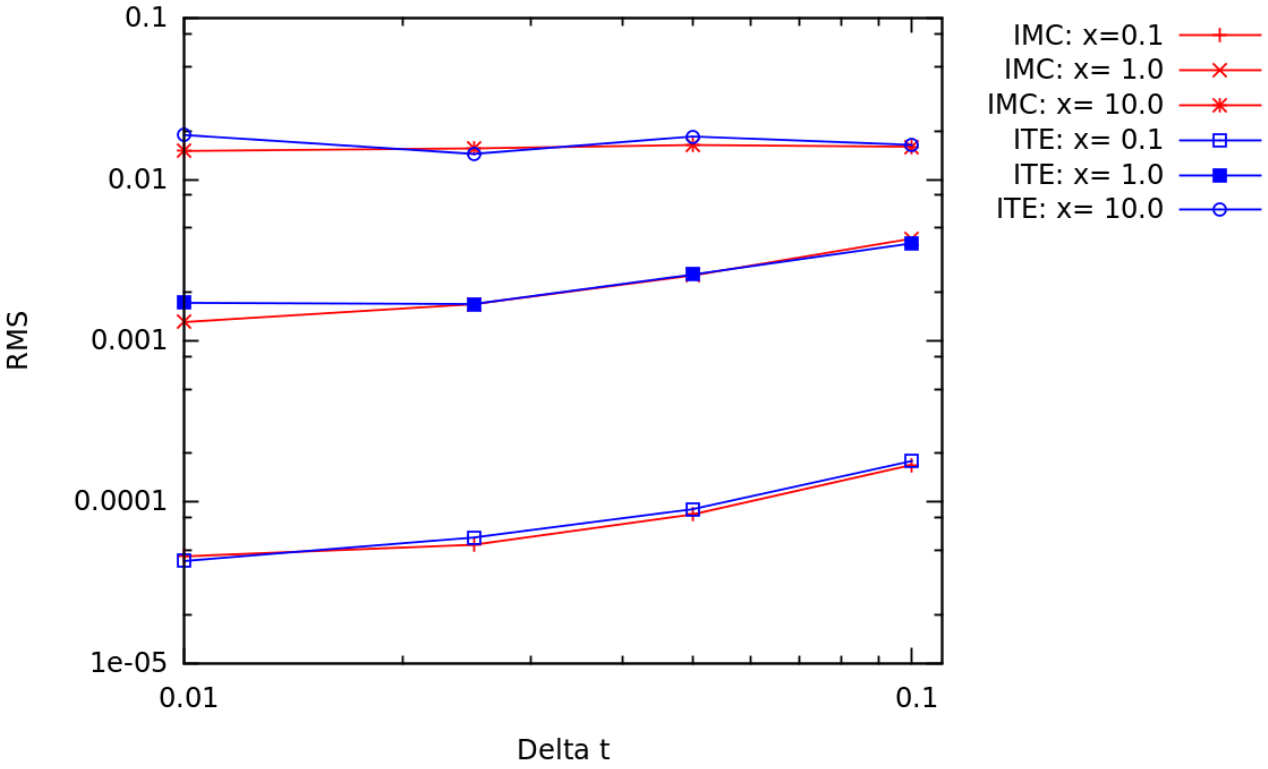

Figure 9: Comparing the RMS error for the IMC and ITE IMC method with four sub-steps at various times in the Su Olson problem

$$\frac{dU}{dt} = f_n \sigma_n c(E - U_r^n). \tag{52}$$

A slight modification is made when using two steps of the ITE IMC method:

$$\frac{dE_1}{dt} + f_1^n \sigma^n c E_1 = f_1^n \sigma^n c U_{1,r}^{n+1}, \tag{53}$$

$$\frac{dU_1}{dt} = f_1^n \sigma^n c(E_1 - U_{1,r}^{n+1}). \tag{54}$$

In the ITE IMC method U_r^{n+1} is estimated using information from the previous sub-steps. For the first sub-step, the ITE IMC method estimates the emission temperature, $U_{r,1}^{n+1}$, with $U_{r,1}^{n+1} = \frac{U_r^n}{2}$. These equations can be solved and evaluated at t_{n+1} to yield:

$$E_1^{n+1} = \frac{1}{2}\left(E^n e^{-f_1^n \sigma^n c(t-t_n)} + U_r^n \left(1 - e^{-f_1^n \sigma^n c \Delta t}\right)\right), \tag{55}$$

$$U_1^{n+1} = \frac{1}{2}\left(U^n + (E^n - U_r^n)\left(1 - e^{-f_1^n \sigma^n c \Delta t)}\right)\right). \tag{56}$$

These equations can be written in a very general form:

$$E_1^{n+1} = \frac{1}{2}AE^n + \frac{1}{2}BU^n \tag{57}$$

$$U_1^{n+1} = \frac{1}{2}(1-A)E^n + \frac{1}{2}(1-B)U^n \tag{58}$$

If two steps are used in the ITE IMC method, the emission temperature for the second sub-step is estimated as $U_{r,2}^{n+1} = \frac{U_{r,1}^{n+1} + U_{r,2}^n}{2}$ and $U_{r,2}^n = \frac{U_r^n}{2}$. The radiation and material energy balance for the second sub-step become

$$\frac{dE_2}{dt} + f_2^n \sigma^n c E_2 = f_2^n \sigma^n c \frac{U_{r,1}^{n+1} + \frac{U_r^n}{2}}{2}, \tag{59}$$

$$\frac{dU_2}{dt} = f_2^n \sigma^n c \left(E_2 - \frac{U_{r,1}^{n+1} + \frac{U_r^n}{2}}{2}\right), \tag{60}$$

where $U_{1,r}^{n+1}$ is now a constant equal to $\beta U_1(t_{n+1})$.

This system of equations is then solved to yield an expression for E_2^{n+1} and U_2^{n+1}:

$$\begin{aligned} E_2^{n+1} = &\left(\frac{1}{2}\gamma_2 + U_{1,E}(\frac{1}{2}\beta - \frac{1}{2}\beta\gamma_2)\right) E \\ &+ \left(\frac{1}{4}\beta - \frac{1}{4}\beta\gamma_2 + U_{1,U}(\frac{1}{2}\beta - \frac{1}{2}\beta\gamma_2)\right) U, \end{aligned} \tag{61}$$

$$\begin{aligned} U_2^{n+1} = &\left(\frac{1}{2} - \frac{1}{2}\gamma_2 - U_{1,E}(\frac{1}{2}\beta - \frac{1}{2}\beta\gamma_2)\right) E \\ &+ \left(\frac{1}{2} - \frac{1}{4}\beta + \frac{1}{4}\beta\gamma_2 - U_{1,U}(\frac{1}{2}\beta - \frac{1}{2}\beta\gamma_2)\right) U. \end{aligned} \tag{62}$$

In Eqs. (61) and (62) $\alpha = -f^n \sigma^n c$ and $\gamma = e^{-\alpha \Delta t}$. β is used to write the equation in terms of U instead of U and U_r. Eqs. (61) and (62) can also be rewritten in a very general form:

$$E_2^{n+1} = \frac{1}{2}A'E^n + \frac{1}{2}B'U^n, \tag{63}$$

$$U_2^{n+1} = \frac{1}{2}(1 - A')E^n + \frac{1}{2}(1 - B')U^n. \tag{64}$$

If more than two sub-steps are used in ITE IMC, the equations for any sub-step can be written in the same general form because the U_r term for any sub-step U_i with $i > 1$ is simply $U_i + c$ where c is a constant equal to the sum of the previously determined emission terms:

$$c = \sum_{j=1}^{i-1} U_{r,j}^{n+1}, \tag{65}$$

where j is an ITE sub-step that has already been determined and i corresponds to the current sub-step.

U^{n+1} and E^{n+1} are determined by summing the values for U_i^{n+1} and E_i^{n+1} over all the sub-steps. Using the general forms of those equations yields

$$E^{n+1} = (A + A')E^n + (B + B')U^n \tag{66}$$

$$U^{n+1} = ((1 - A) + (1 - A'))\, E^n + ((1 - B) + (1 - B'))\, E^n \tag{67}$$

This system of equations again simplifies to the form:

$$E^{n+1} = CE^n + DU^n \tag{68}$$

$$U^{n+1} = (1 - C)E^n + (1 - D)U^n \tag{69}$$

Any 2 x 2 system of equations that can be written in this form will have the same eigenvalues:

$$\lambda_1 = 1, \lambda_2 = C - D. \tag{70}$$

The stability can then be determined such that $|C - D|$ is maintained less than unity. The ITE method for an arbitrary number of steps results in an equation

like Eqs. (68) and (69) and thus the ITE method eigenvalues always have the same form.

An expression for $|C - D|$ can be determined for any number of sub-steps when using the ITE method in 0-D. Consider sub-step i of an ITE method with N sub-steps:

$$\frac{dE_i}{dt} + f_i^n \sigma^n c E_i = f_i^n \sigma^n c U_{r,i}^{n+1}, \tag{71}$$

$$\frac{dU_i}{dt} = f_i^n \sigma^n c (E_i - U_{r,i}^{n+1}), \tag{72}$$

where $U_{r,i}^{n+1}$ is now a function of all the previous time steps:

$$U_{r,i}^{n+1} = \frac{U_{r,1}^{n+1} + U_{r,2}^{n+1} + ... + U_{r,i-1}^{n+1} + \frac{(N-i)U_r^n}{N}}{N}. \tag{73}$$

The equations for E_i^{n+1} and U_i^{n+1} are:

$$E_i^{n+1} = \left(\frac{1}{N}\gamma_i + U_{C,E}(\frac{1}{N}\beta - \frac{1}{N}\beta\gamma_i)\right) E$$

$$+ \left(\frac{N-i+1}{N^2}\beta - \frac{N-i+1}{N^2}\beta\gamma_i + U_{C,U}(\frac{1}{N}\beta - \frac{1}{N}\beta\gamma_i)\right) U, \tag{74}$$

$$U_i^{n+1} = \left(\frac{1}{N} - \left(\frac{1}{N}\gamma_i + U_{C,E}(\frac{1}{N}\beta - \frac{1}{N}\beta\gamma_i)\right)\right) E$$

$$+ \left(\frac{1}{N} - \left(\frac{N-i+1}{N^2}\beta - \frac{N-i+1}{N^2}\beta\gamma_i + U_{C,U}(\frac{1}{N}\beta - \frac{1}{N}\beta\gamma_i)\right)\right) U, \tag{75}$$

where

$$U_{C,E} = U_{1,E} + U_{2,E} + ... + U_{i-1,E}, \tag{76}$$

and

$$U_{C,U} = U_{1,U} + U_{2,U} + ... + U_{i-1,U}. \tag{77}$$

These U_C values represent the coefficients in front of E and U in each U_i equation (E_i equations are only used when calculating the total E^{n+1}). The $N - i + 1$ terms come from the addition of the $U_{i+1}...U_N$ values that have not yet been determined

and are thus approximated as $\frac{U_r^n}{N}$. Because U_i and E_i depend on all the previous sub-steps, Eqs. (74) and (75) can be used recursively to find the numerical values of the coefficients for U_i and E_i. When $i = 1$, Eqs. (55) and (56) are used to calculate the coefficients. The stability of the system is determined from $|C - D| < 1$ where C and D are:

$$C = (E_{1,E} + E_{2,E} + ... + E_{N-1,E} + E_{N,E}), \tag{78}$$

$$D = (E_{1,U} + E_{2,U} + ... + E_{N-1,U} + E_{N,U}), \tag{79}$$

where $E_{i,E}$ and $E_{i,U}$ are coefficients multiplying the respective E and U terms in the E_i^{n+1} equation.

5.3.1 Numerical Results

The second eigenvalue, λ_2, was numerically calculated with $a = c = \sigma = 1$ and $\beta = 3$ for various values of Δt. The results are shown in Figure (10). For all values of Δt, $|\lambda_2| < 1$ and for $\Delta t < 2.1$ the solution is monotonic ($0 < \lambda_2 < 1$). The ITE IMC method is monotonic over the same time step range as the standard IMC method. For time steps greater than 2.1, the eigenvalue decreases slightly as more ITE sub-steps are used. IMC and ITE IMC simulations were performed for $\Delta t = 0.235$ and $\Delta t = 50.0$ with an initial radiation density $E_0 = 1000$ and an initial material energy density $U_0 = 0.0$. Figures (11) through (13) show E and U as a function of time. Figure (11) shows that for positive eigenvalues, IMC and ITE IMC generate solutions that compare very well with the predicted solution and with each other (they have the same λ_2). For $\Delta t = 50.0$, the IMC and ITE IMC simulation values again compare well with the predicted values. In Figure (13), the smaller predicted λ_2 value for the ITE IMC method with four sub-steps is evident in the slightly less oscillatory nature of the solution.

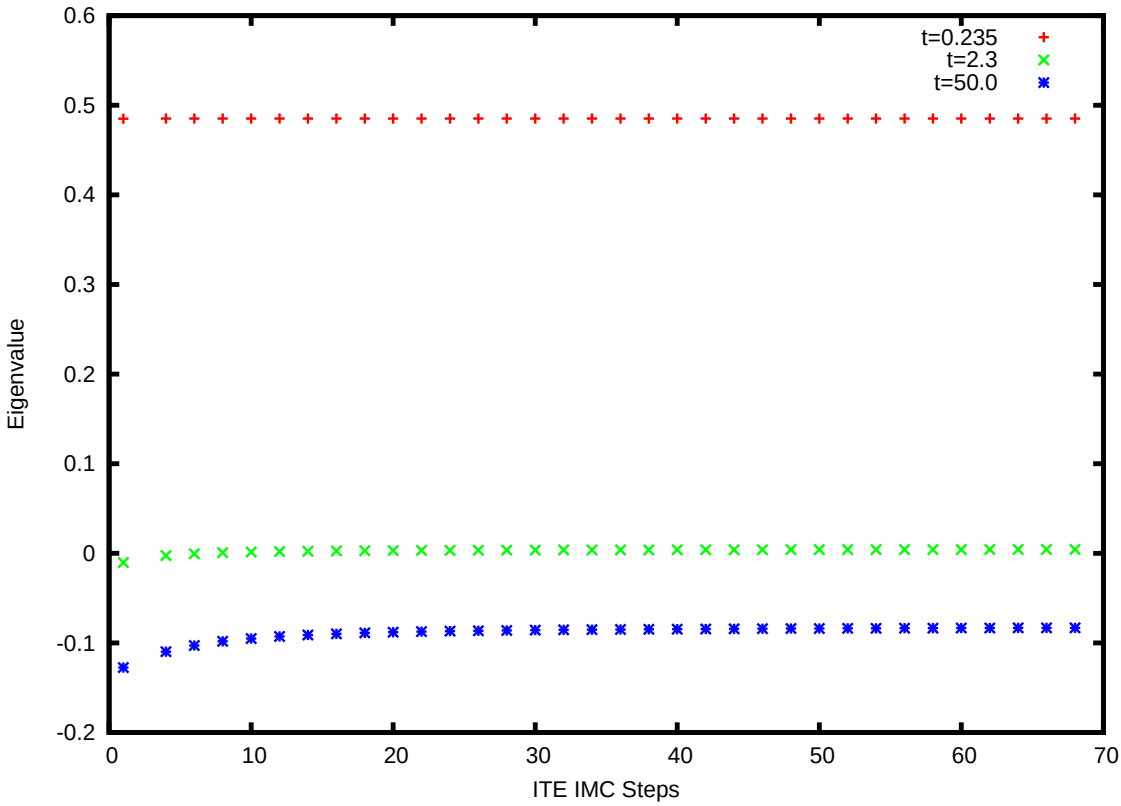

Figure 10: λ_2 values vs. ITE IMC steps for various Δt values

5.3.2 Teleportation Error

The teleportation error associated with ITE IMC method was determined using the method presented by Cheatham [3]. This test problem is grey and 1D with $c_V = 4.0T^3$, $a = c = 1.0$ (the problem is unitless) and $\sigma = 100.0$. Vacuum boundary conditions are imposed on both sides and a plane source of 1.0 is placed at the left boundary. The results are compared at $t = 10.0$ with an IMC simulation that used $\Delta x = 0.01$ and $\Delta t = 0.05$. To investigate the behavior of the teleportation error, Δx will be increased relative to the reference solution or Δt will be decreased.

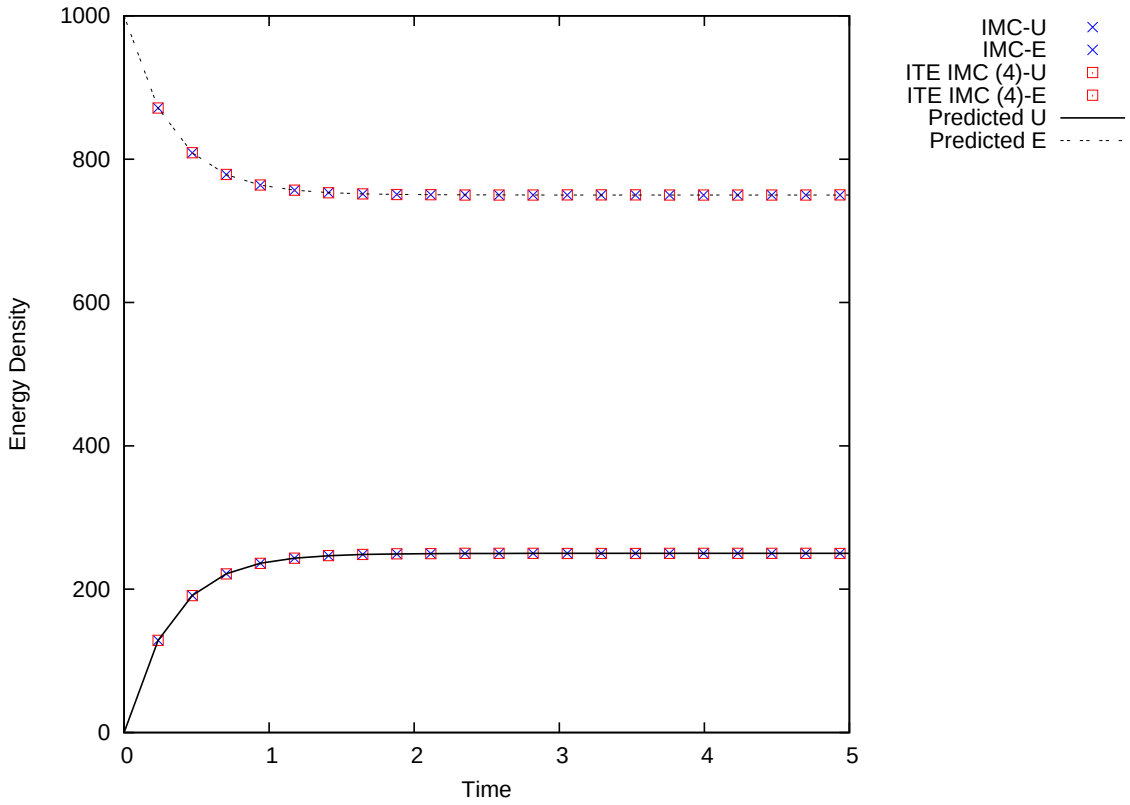

Figure 11: Radiative and material energy density vs. time for $\Delta t = 0.235$

Figure (14) shows how energy is transferred further into the problem as Δt is decreased. The ITE IMC method has a higher material temperature relative to the reference solution. Photon teleportation results because the emission location of a photon is sampled uniformly over a cell. The ITE IMC method emits photons multiple times during a time step, which means that uniform position sampling occurs multiple times during a time step. Figure (15) compares the teleportation error for different numbers of ITE IMC sub-steps. As the number of sub-steps is increased, the overheating due to teleportation also increases. The teleportation

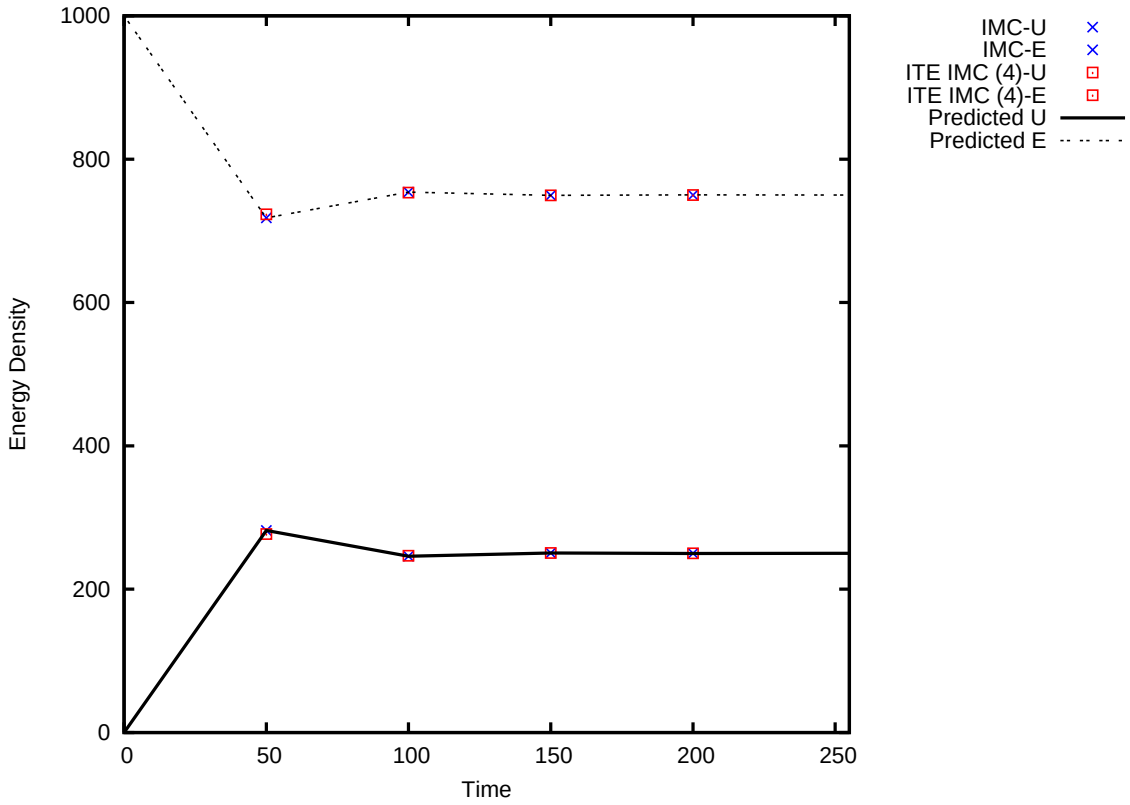

Figure 12: Radiative and material energy density vs. time for $\Delta t = 50.0$

error does not increase indefinitely as ITE IMC sub-steps are increased. This is likely because at some point the amount of energy traveling faster than light is negligible.

5.4 Marshak Wave

The ITE IMC method is especially useful in Marshak wave problems, where violations of the maximum principle are most likely to occur. The Marshak wave problem from Larsen and Mercier's paper [13] was simulated with both IMC and

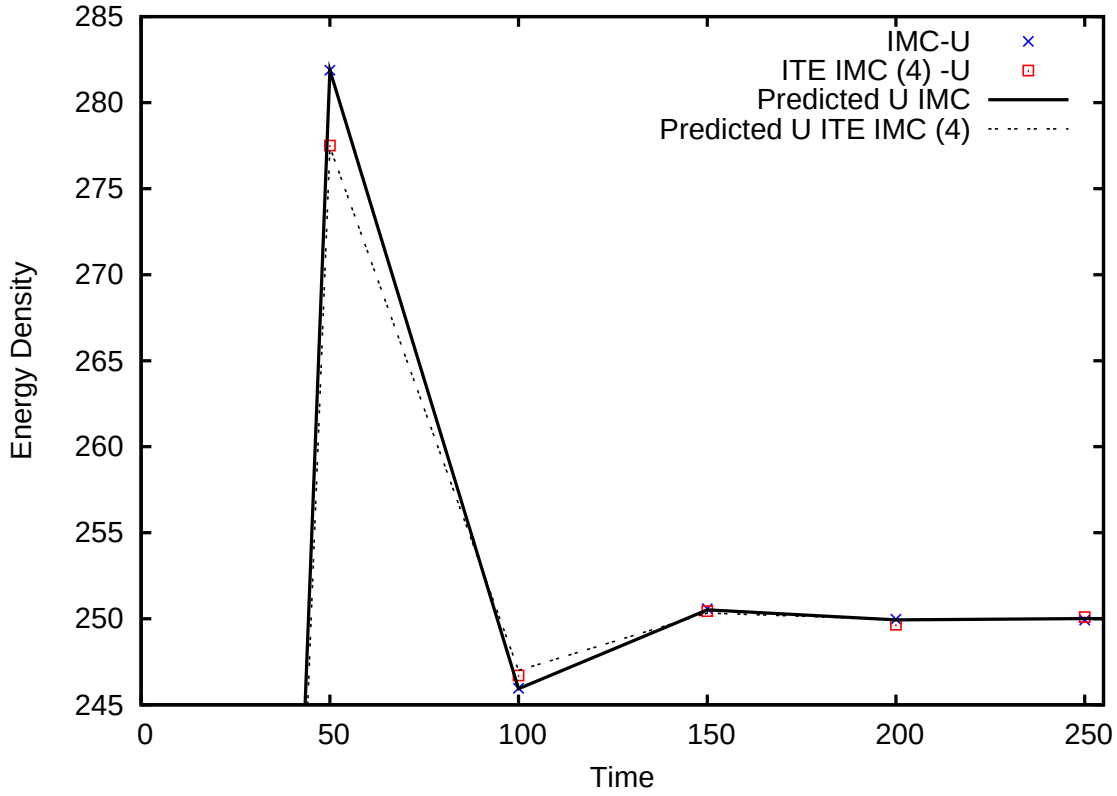

Figure 13: Material energy density vs. time for $t = 50.0$ showing the different λ_2 value for IMC and ITE IMC methods

ITE IMC methods. In the Marshak wave problem, the opacity is proportional to $\frac{1}{T^3}$, meaning that cold regions will have a very small mean free path. As the material heats up it becomes more transparent to photons. The IMC method does not update its temperature dependent properties during the time step and so the cold material will be very opaque throughout the time step and too much energy will be absorbed if the time step is relatively large. The ITE IMC method updates the temperature dependent properties at the end of each sub-step, thus allowing the material to become more transparent throughout the time step.

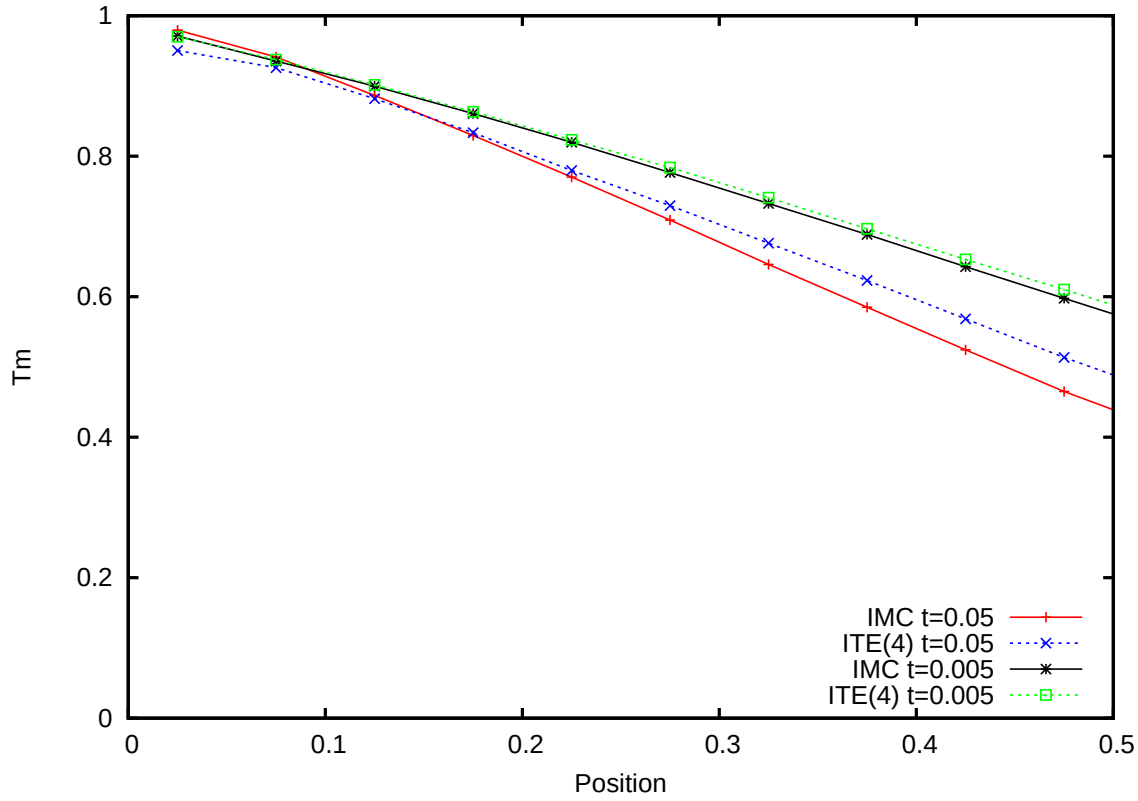

Figure 14: Material Temperature vs. position in teleportation problem for IMC and ITE IMC at $t = 10.0$

The IMC and ITE IMC simulations were used the physical parameters and boundary conditions from the following table:

$$\begin{aligned} \sigma_a(T) &= \frac{15}{\pi^4}\frac{27}{T^3} \\ c_V &= 0.0081181 \ \frac{\text{jk}}{\text{keVcm}^3} \\ T_0 &= 0.001 \text{ keV} \\ T_B &= 1.0 \text{ keV} \\ c &= 300.0 \ \frac{\text{cm}}{\text{shake}} \\ a &= 0.013720160 \ \frac{\text{jk}}{\text{cm}^3\text{keV}^4} \end{aligned}$$

Results at various temporal points in the problem are shown in Figures (16) and (17). Both figures show that the ITE IMC method allows more energy to

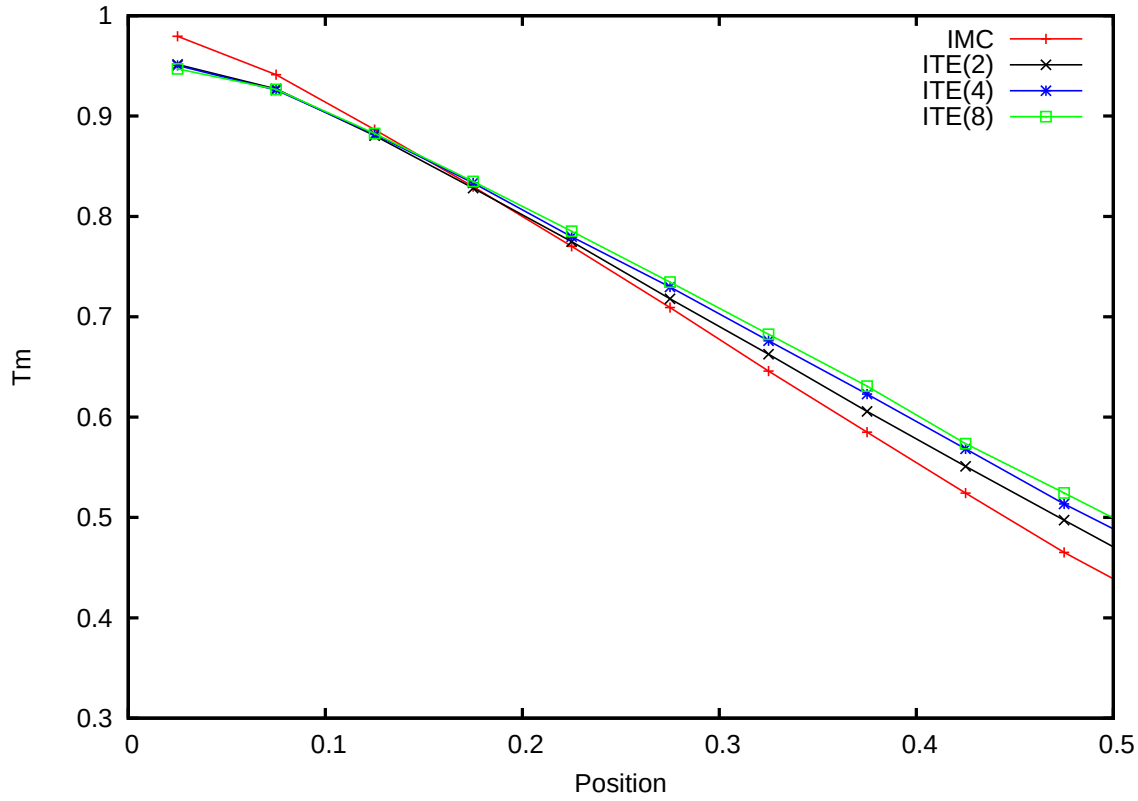

Figure 15: Material temperature vs. position for $\Delta t = 0.05$ at $t = 10.0$ for the ITE IMC method with varying number of sub-steps

enter the problem while maintaining all material temperatures below the boundary temperature.

A script was developed to determine the conditions under which IMC and ITE IMC first violate the maximum principle: the Marshak wave problem was simulated with constant grid spacing and a small time step. The time step was gradually increased until a violation of the maximum principle occurred. This procedure was used to generate the data in Figure (18). Figure (18) shows that

the ITE IMC method always allows for larger time steps without violating the maximum principle for any level of grid spacing. The longer time steps allowed by the ITE IMC method come at the expense of an increased variance in the material temperature.

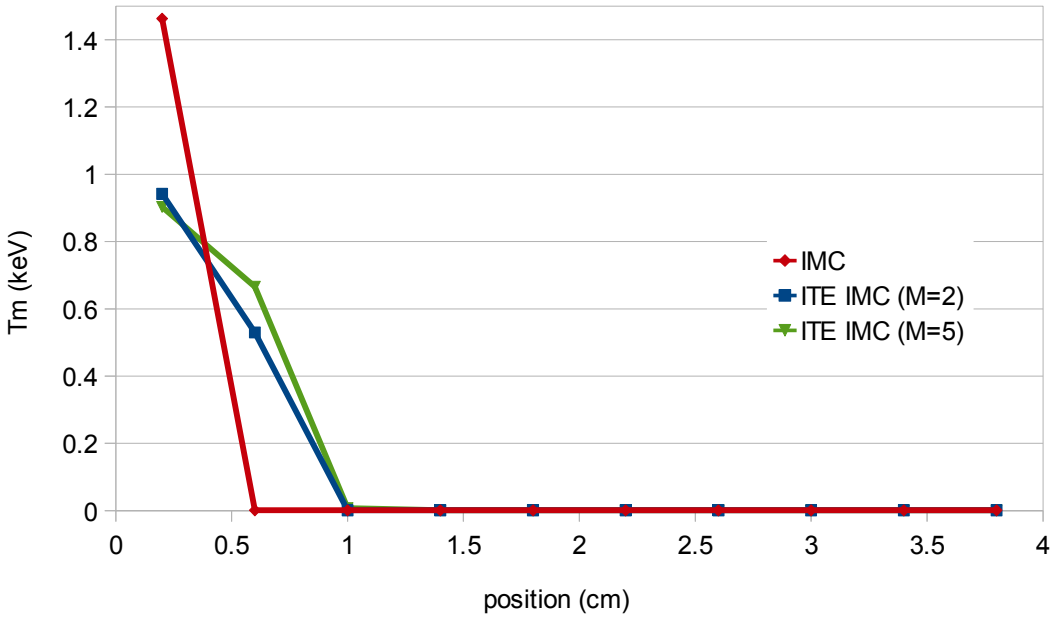

Figure 16: Material temperature vs. position at the end of one time step where $\Delta t = 0.04$ shakes and $\Delta x = 0.4$ cm

5.5 Crooked Pipe Problem

The crooked pipe test problem was designed by Graziani and LeBlanc in 2000 [9]. Its purpose is to test the validity of radiation transport codes in non-diffusive conditions. In the crooked pipe problem there are two types of material regions: an optically thin region with a lower heat capacity and an optically thick region with a high heat capacity. The thin region is the pipe and it is embedded within the thick material. The problem described by Graziani and LeBlanc is solved in

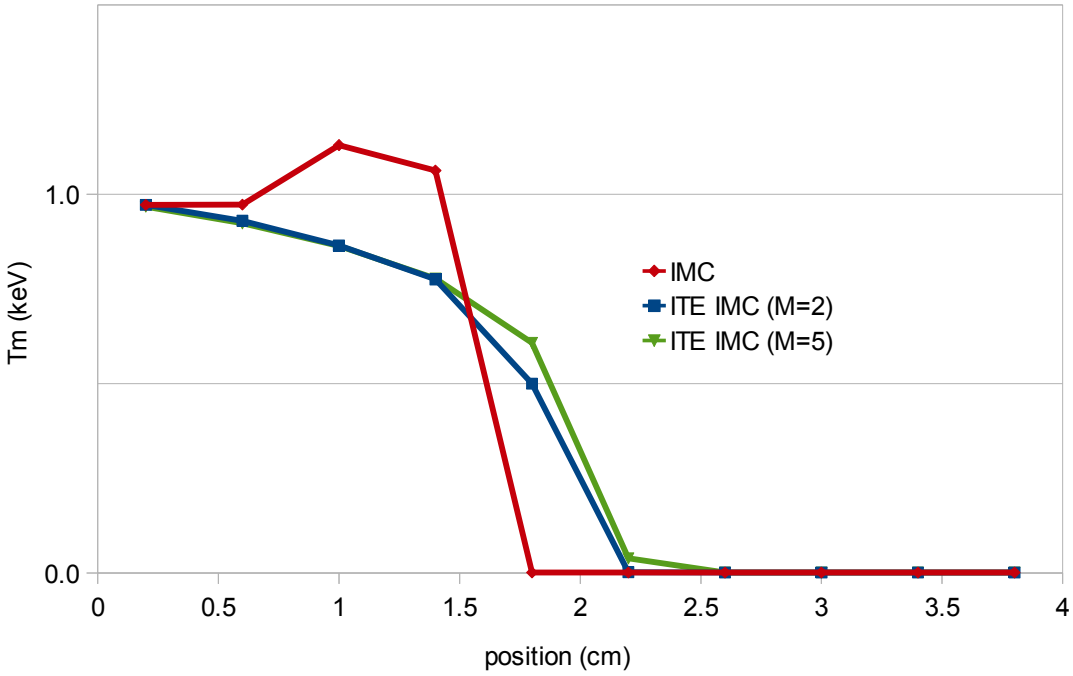

Figure 17: Material temperature vs. position after at $t = 0.16$ shakes where $\Delta t = 0.04$ shakes and $\Delta x = 0.4$ cm

curvilinear r-z geometry: we consider a Cartesian, x-y geometry version. The pipe has four 90 degree turns as it runs from $x = 0$ to $x = 7.0$ cm. Radiation cannot travel around corners because it does not diffuse. In a scattering medium it can be described with diffusion equations but in optically thin systems this assumption is not valid. A 0.5 keV source is placed at $x = 0$ and vacuum boundaries are imposed at $x = 0$, $y = 2.0$ cm and $x = 7.0$ cm. We impose a reflecting boundary at $y = 0$.

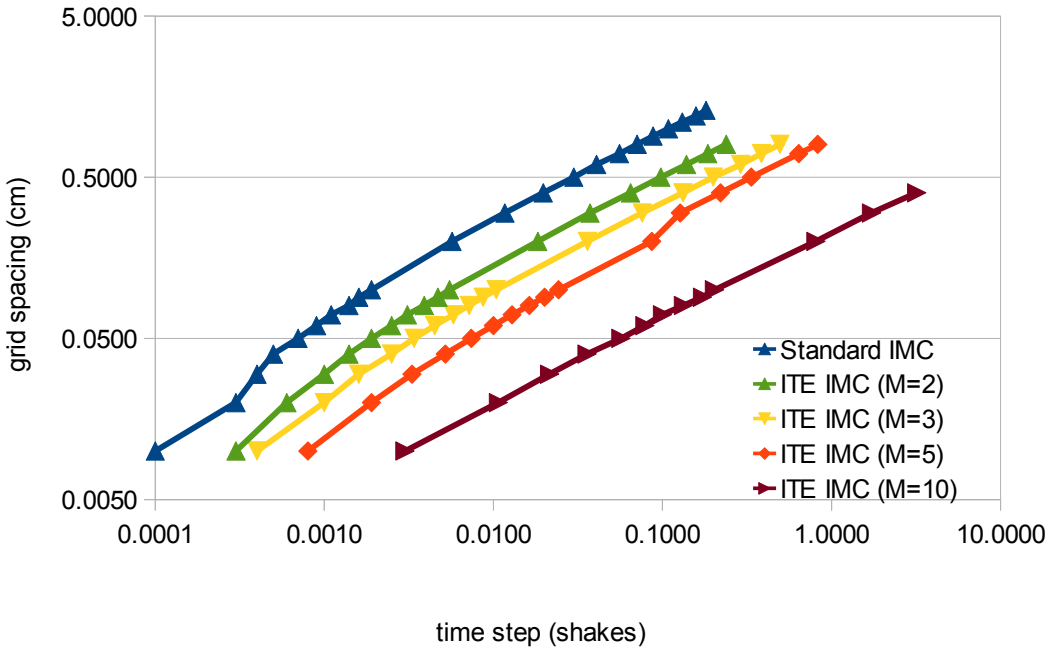

Figure 18: First violations of the maximum principle for Standard IMC and the ITE IMC Method

Other parameters are shown in the following table:

σ_{thick}	=	2000 cm^{-1}
σ_{thin}	=	0.2 cm^{-1}
$c_{V\,thick}$	=	0.1 $\frac{\text{jk}}{\text{keVcm}^3}$
$c_{V\,thin}$	=	0.0001 $\frac{\text{jk}}{\text{keVcm}^3}$
T_0	=	0.05 keV
T_B	=	0.5 keV
Δt	=	0.001 shakes
Photons	=	50000
c	=	300.0 $\frac{\text{cm}}{\text{shake}}$
a	=	0.013720160 $\frac{\text{jk}}{\text{cm}^3\text{keV}^4}$

The temperature is plotted at 5 points within the "pipe": Point 1: $x = 0.25$ cm, $y = 0$, Point 2: $x = 2.75$ cm, $y = 0$, Point 3: $x = 3.5$ cm, $y = 1.25$ cm, Point 4: $x = 4.25$ cm, $y = 0$, and Point 5: $x = 6.75$ cm, $y = 0$ cm.

A heat map that illustrates the geometry of the crooked pipe problem is shown

for the ITE method with 4 sub-steps in Figure (19). In Figure (20) the IMC and ITE IMC results are compared side by side. Figure (21) shows the temperature at the 5 points for the IMC and ITE IMC methods. The larger variance with time is expected because as more energy enters the problem the same number of photons are used to simulate that energy so each zone on the mesh will receive less photons. Figure (21) also shows a rough agreement between IMC and ITE IMC in the crooked pipe problem. The large variance in material temperature present in the ITE IMC method is visible in Figure (20). The ITE IMC temperature slightly lags behind the IMC solution, possibly due to teleportation into the opaque material.

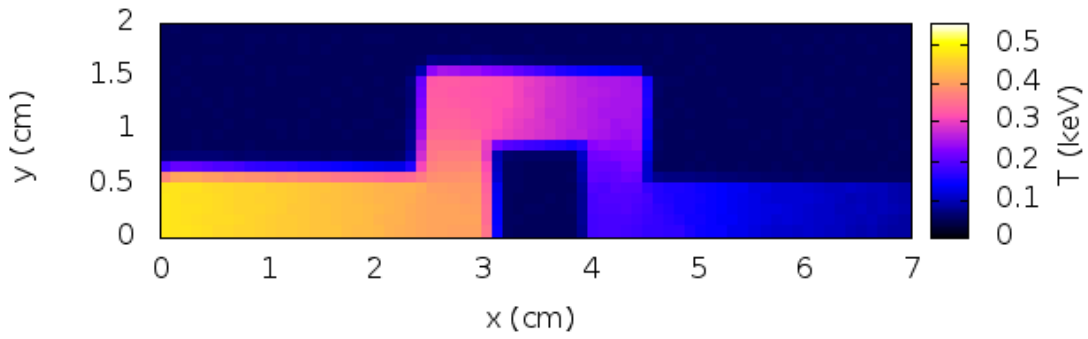

Figure 19: Material temperature vs. position for the ITE IMC method at $t \approx 4.0sh$

5.6 Figure of Merit

The figure of merit (FOM) for Monte Carlo problems is defined by the variance of the result and the run time:

$$FOM = \frac{1}{t\sigma^2}, \tag{80}$$

where σ^2 is the variance of the answer (usually the material or radiation temperature) and t is the run time. Shorter run times and smaller variance yields a larger FOM.

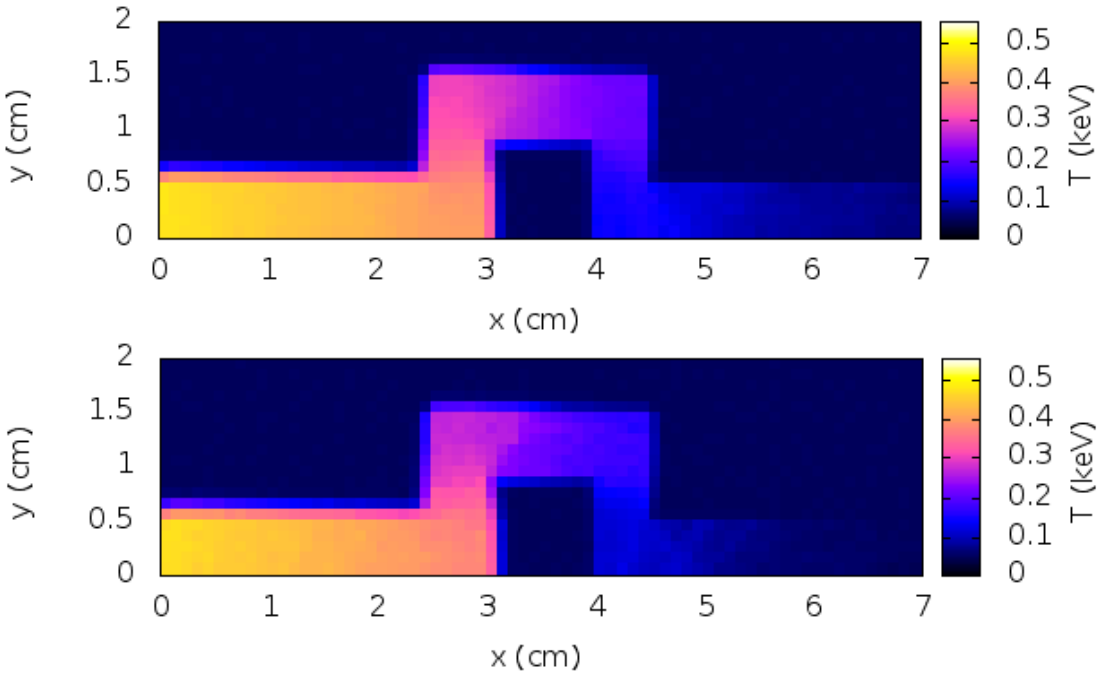

Figure 20: Material temperature vs. position at $t = 2.5$ shakes for IMC (top) and ITE IMC (bottom)

The variance of the material temperature of a zone in the IMC method is related to the variance of the absorption tally, I.

$$\sigma^2(T) = \frac{1}{N-1}(\frac{1}{N}\sum_{i=1}^{N} I_i^2 - I^2). \tag{81}$$

Where I_i is the energy deposited in one event and I is the total energy absorbed. The material temperature variance for a zone in ITE IMC method is:

$$\sigma_T = \sum_{k=1}^{K}(\frac{1}{c_V V_{cell}}\sigma_I)^2. \tag{82}$$

K is the total number of ITE sub-steps V_{cell} is the volume of the mesh zone.

To compare the FOM for the IMC and ITE IMC methods, both methods were used to solve the 0-D problem from Mosher [17]. In both problems $a = c = 1.0$ so the time and temperature are unitless. The same problem parameters were used in the FOM test and the 0D verification test but the IMC method used $\Delta t = 0.1$ and

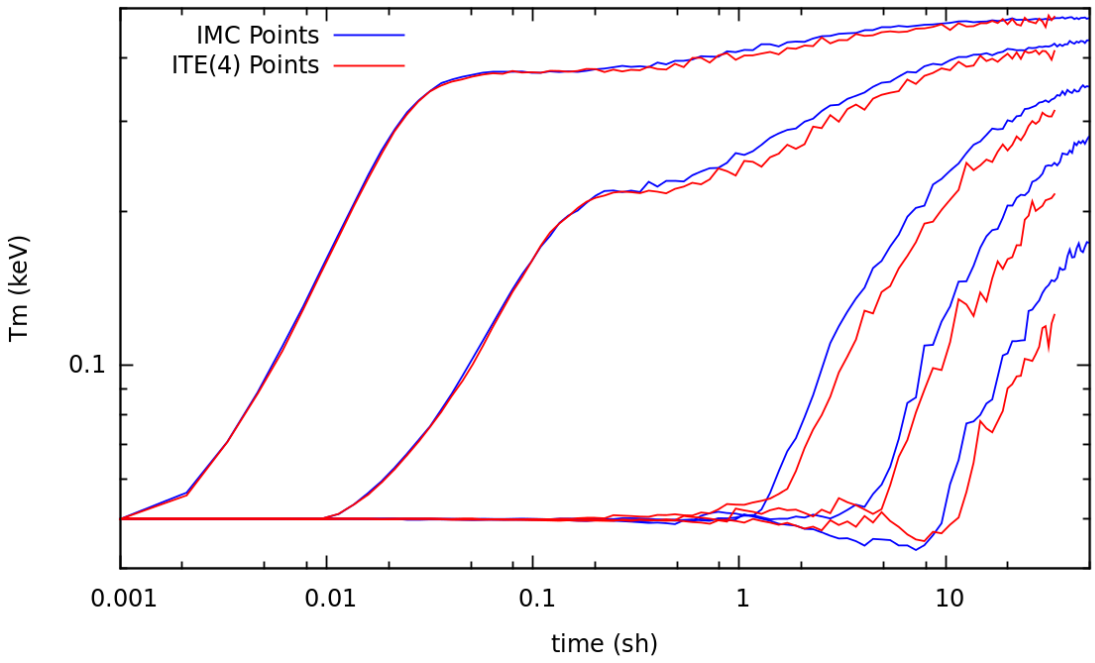

Figure 21: Material temperature vs. time for the five examined points in crooked pipe problem

the ITE method with 4 sub-steps used $\Delta t = 0.3$. These values correspond to the smallest time step that does not violate the maximum principle for each method. The problem was simulated ten times with 100000 photons and the variance was compared at $t = 0.12$. Table (1) shows the results of the FOM test. Fig. (22) shows that the IMC method overheats when $\Delta t = 0.3$ is used.

When parts of the problem are near equilibrium the Fleck factor does not vary with time. In these conditions the ITE IMC Fleck factor, found in Eq. (43), will be equal to the IMC Fleck factor in the first sub-step and less than the IMC Fleck factor for all other sub-steps. This means that the ITE IMC will have less effective scattering at near equilibrium conditions and will run faster than traditional IMC. An infinite medium problem was run with the matter and radiation at equilibrium with $T_m = 2.0$ keV. The problem was run with 4 ITE sub-steps, $\Delta t = 1.0$ sh,

Method	Run Time (s)	Variance	FOM
IMC	3.691	9.085 E-10	2.98 E8
ITE(4)	1.207	8.8974 E-9	9.31 E7

Table 1: Results for FOM test, average of ten runs

Method	Run Time (s)	Avg. Fleck Factor	Variance	FOM
IMC	49.94	0.7072	8.172 E-11	2.45 E8
ITE(4)	42.74	0.1318	8.868 E-10	2.64 E7

Table 2: Results for equilibrium FOM test, average of three runs

t_{end} = 10 sh and 100000 photons. The variance and run time are compared in Table (2). The average Fleck factor listed in Table (2) represents the average of the four different Fleck factors that result from each of four sub-steps of ITE IMC. Figure (23) shows the results of the 0D problem and the variance associated with the ITE IMC.

5.7 Summary

The ITE IMC method has been shown to correctly solve common TRT test problems. The stability of the method was also explored and found to be similar to the IMC method. ITE IMC was shown to allow larger time steps for Marshak wave problems and it physically allows energy to penetrate further into the problem. The figure of merit for the ITE IMC method was found to be smaller than the IMC method.

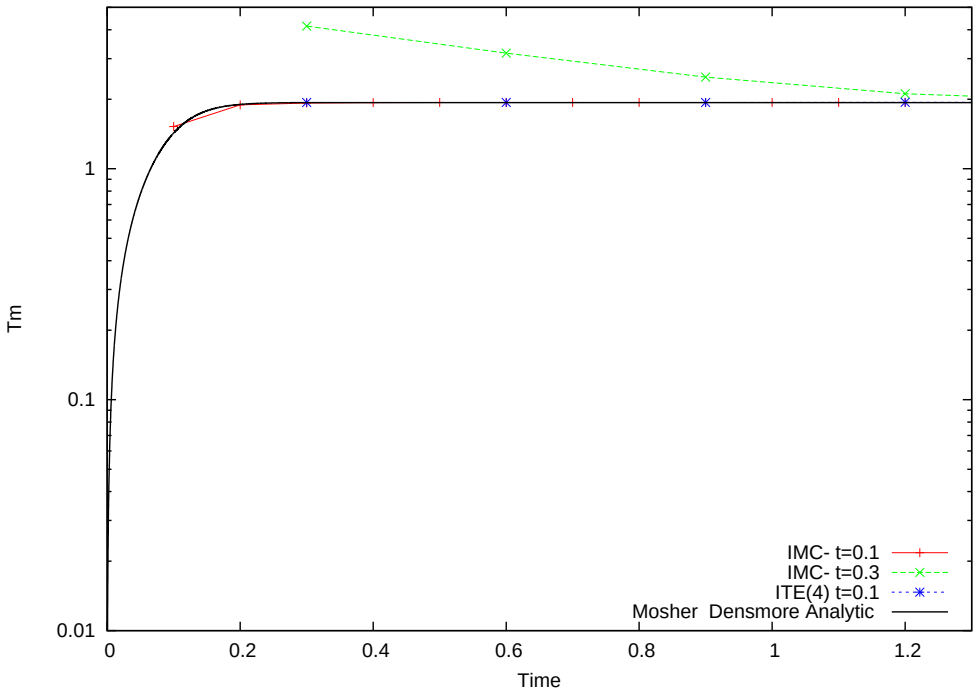

Figure 22: Material temperature vs. time showing overheating with IMC in Mosher 0D test problem

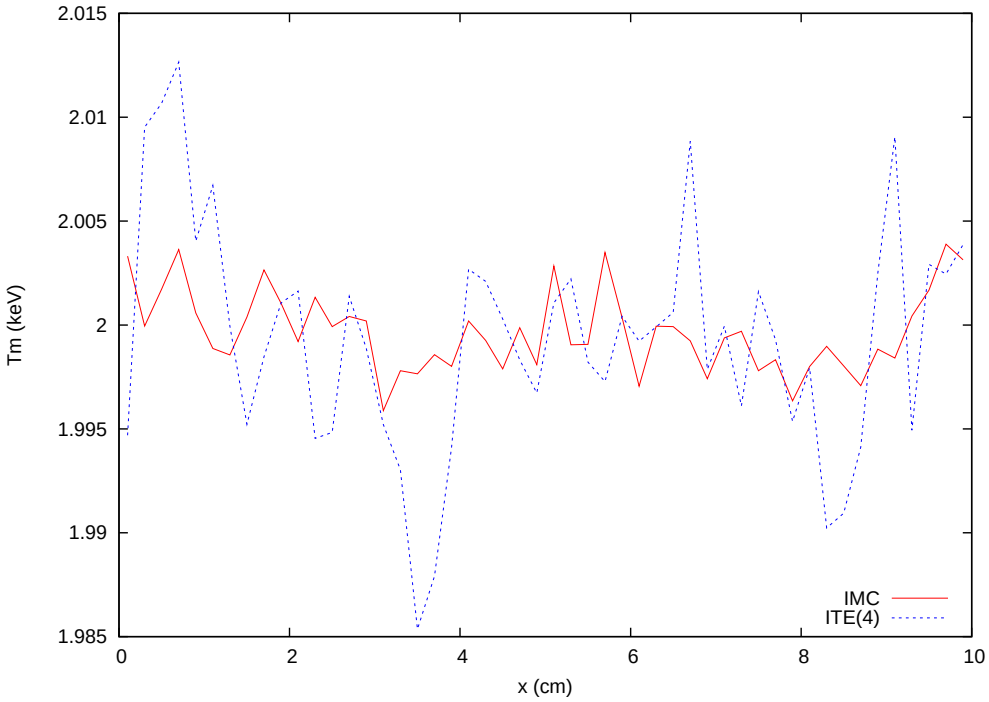

Figure 23: Material temperature vs. position for IMC and ITE IMC in an infinite medium problem at equilibrium

6 Conclusions

6.1 Introduction

The ITE IMC method has been shown to obey the maximum principle for a wider range of problem parameters than standard IMC. It has been validated in 0-D, 1-D and 2-D problems and with linear and non-linear problem parameters. The teleportation problem present in IMC simulations is exacerbated with the use of ITE IMC. The envelope of time steps that obey the maximum principle for the Marshak wave problem has been mapped.

6.2 Iterative Thermal Emission IMC

To evaluate the results, the ITE IMC method is compared with traditional IMC, which is the standard for Monte Carlo photon transport. The ITE IMC method presents one possible solution to the overheating problem present in IMC simulations. By using more sub-steps of the ITE IMC method, the simulation can be performed using larger time steps without violating the maximum principle and the end result can be obtained more quickly. Currently, the variance of the ITE IMC method will always be larger than the IMC results when the same number of particles are used. This is because several energy absorption tallies are combined in ITE IMC compared to the single absorption tally in the IMC method. The ITE IMC method has a different Fleck factor than standard IMC and if part of the problem is near equilibrium the ITE IMC method will always have a smaller Fleck factor and thus less effective scattering. This smaller Fleck factor leads to faster run times for ITE IMC of about 14% in an infinite medium test problem

at equilibrium. In problems where large zones are used, the teleportation error manifested as higher temperatures further into a 1D problem, is larger when ITE IMC is used. The teleportation error is made worse when more ITE sub-steps are used.

6.3 Overall Conclusions and Future Work

The ITE IMC method can be used to reduce overall simulation time by allowing longer time steps without violating the maximum principle. The reduced run time comes at the cost of an increase in variance relative to the IMC method. Future work could be done to improve the variance and teleportation errors associated with ITE IMC. Variance reduction techniques like global weight windows [25] and symbolic weights [11] could be used with ITE IMC method to reduce variance. There are several methods for correcting teleportation error and their efficacy with the IMC method has been tested [3]. These methods could be useful in reducing teleportation error in ITE IMC simulations.

ITE IMC provides a larger stability envelop for Marshak wave problems. Currently work is being done to characterize the time step limits on other common TRT problems. ITE IMC could prove to be even more useful at reducing overheating in other classes of problems. The ITE IMC method could also be implemented in 3D and tested on benchmark problems in that geometry.

Bibliography

[1] J.P. Apruzese and J.L. Giuliani. Multi-dimensional radiation transport for modeling axisymmetric z pinches: Ray tracing compared to monte carlo solutions for a two-level atom. *Journal of Quantitative Spectroscopy and Radiative Transfer*, 111(1):134 – 143, 2010.

[2] L. L. Carter and C. A. Forest. Nonlinear radiation transport simulation with an implicit monte carlo method. Technical Report LA-5038, Los Alamos National Laboratory, 100, 1973.

[3] J. R. Cheatham. *Truncation Analysis and Numerical Method Improvements for the Thermal Radiative Transfer Equations.* PhD thesis, University of Michigan, Ann Arbor, Michigan, 2010.

[4] R. Eckhardt. Stan ulam, john von neumann, and the monte carlo method. *Los Alamos Science*, 15:131–143, 1987.

[5] J. A. Fleck. The calculation of nonlinear radiation transport by a monte carlo method. *Methods in Computational Physics*, 1:46–65, 1963.

[6] J. A. Fleck and J. D. Cummings. An Implicit Monte Carlo scheme for calculating time and frequency dependent nonlinear radiation transport. *J. Comp. Phys.*, 8:313–342, 1971.

[7] N.A. Gentile. A comparison of various temporal discretization schemes for infinite media radiation transport. *Trans. Am. Nucl. Soc.*, 97:544 – 546, 2007.

[8] N.A. Gentile. Including the effects of temperature-dependent opacities in the implicit monte carlo algorithm. *J. Comp. Phys.*, 230(12):5100 – 5114, 2011.

[9] F. Graziani and J. LeBlanc. The crooked pipe test problem. Technical Report UCRL-MI-143393, Lawrence Livermore National Laboratory, 100, 2000.

[10] G. Y. Han and Y. J. Cho. Radiative heat transfer in a circulating fluidized bed coal combustor. *Powder Technology*, 102(3):266 – 273, 1999.

[11] Eugene D Brooks III. Symbolic implicit monte carlo. *Journal of Computational Physics*, 83(2):433 – 446, 1989.

[12] F. P. Incropera, D. P. DeWitt, Bergman T.L., and Adrienne S.L. *Fundamentals of heat and mass transfer-6th ed.* John Wiley & Sons Inc., New York, 6th edition, 2007.

[13] Edward W. Larsen and Bertrand Mercier. Analysis of a Monte Carlo method for nonlinear radiative transfer. *J. Comp. Phys.*, 71:50–64, 1987.

[14] E. E. Lewis and Jr. D. P. Miller. *Computational Methods of Neutron Transport*. American Nuclear Society, Inc., Illinois, 1993.

[15] R. G. McClarren and T. J. Urbatsch. A modified implicit monte carlo method for time-dependent radiative transfer with adaptive material coupling. *J. Comp. Phys.*, 228(16):5669 – 5686, 2009.

[16] E. I. Moses. The national ignition facility (nif): A path to fusion energy. *Energy Conversion and Management*, 49(7):1795 – 1802, 2008. ICENES2007, 13th International Conference on Emerging Nuclear Energy Systems, June 38, 2007, Istanbul, Turkiye.

[17] S.W. Mosher. Exact solution of a nonlinear, time-dependent, infinite-medium, grey radiative transfer problem. *Trans. Am. Nucl. Soc.*, 95:744–747, 2006.

[18] G. C. Pomraning. *The Equations of Radiation Hydrodynamics*. Pergamon, Oxford, 1973.

[19] G.C. Pomraning. The non-equilibrium marshak wave problem. *Journal of Quantitative Spectroscopy and Radiative Transfer*, 21(3):249 – 261, 1979.

[20] William H. Press, Saul A. Teukolsky, William T. Vetterling, and Brian P. Flannery. *Numerical Recipes: The Art of Scientific Computing*. Cambridge University Press, New York, 3rd edition, 2007.

[21] K. M. Blundell S. J. Blundell. *Concepts in thermal physics*. Oxford University Press, Oxford, 2nd edition, 2010.

[22] G. Scheffknecht, L. Al-Makhadmeh, U. Schnell, and J. Maier. Oxy-fuel coal combustiona review of the current state-of-the-art. *International Journal of Greenhouse Gas Control*, 5, Supplement 1(0):S16 – S35, 2011.

[23] B. Su and G. L. Olson. An analytical benchmark for non-equilibrium radiative transfer in an isotropically scattering medium. *Annals of Nuclear Energy*, 24(13):1035 – 1055, 1997.

[24] J.D. Densmore S.W. Mosher. Stability and monotonicity conditions for linear, grey, 0-d implicit monte carlo calculations. *Trans. Am. Nucl. Soc.*, 93:520–522, 2005.

[25] A. B. Wollaber. *Advanced Monte Carlo Methods for Thermal Radiation Transport*. PhD thesis, University of Michigan, Ann Arbor, Michigan, 2008.

[26] Y. P. Zel'dovich and Y.P. Raizer. *Physics of Shock Waves and High-Temperature Hydrodynamic Phenomena*. Academic Press, New York, 1966.